AN ABSTRACT OF THE THESIS OF

Nicole L. LeBlanc for the degree of Master of Science in Veterinary Science presented on August 12, 2014.

Title: Quantitative Evaluation of Left Atrial Volume and Function by One-dimensional, Two-dimensional, and Three-dimensional Echocardiography in a Population of Normal Dogs

Abstract approved:

Katherine F. Scollan

Linear M-mode (1D) and later 2-dimensional (2D) measurements of the left atrium (LA) are commonly been used to assess LA size in veterinary studies despite the fact that studies in human subjects have shown that LA volume (LAV) more accurately reflects LA size than linear measurements due to the complex geometry of the LA. The primary goal of this study was to assess and compare LA size in a population of normal dogs using transthoracic M-mode (1D), 2D, and three-dimensional (3D) echocardiographic techniques. In addition, this study was designed to assess left atrial size at three different

points in the cardiac cycle in order to characterize left atrial function in terms of dimensional changes at the beginning and end of ventricular and atrial systole.

Forty clinically normal dogs of various breeds were stratified into one of four groups (10 dogs <10 kg, 10 dogs=10-25 kg, 10 dogs=25-40 kg, and 10 dogs>40 kg). Complete echocardiographic examinations were obtained on all dogs; dogs with exceedingly poor image quality precluding measurement were excluded from analysis. LAV was estimated by converting linear measurements (average of 3 beats) derived from M-mode and 2D images into LAV using cube and sphere formulas from the right parasternal short axis view at the heart base. LAV was also estimated by the monoplane Simpson's method of disks (MOD), monoplane and biplane area-length method (ALM) from left apical 4- and 2-chamber views. Three-dimensional volume data was derived from 3 different image sets obtained over 4 cardiac cycles from both the right parasternal and left apical imaging planes. Each cardiac cycle was further stratified into 3 conventionally defined LAV; maximum LAV (reservoir phase), minimal LAV (systolic phase), and pre-atrial contraction LAV (conduit phase). Using these volumes, various functional indices were obtained. These included the LA expansion index, total LA emptying volume/fraction, passive LA emptying volume/fraction, and active LA emptying volume/fraction.

The results of this study indicate that different methods of LA measurement are not all comparable. The M-mode derived estimates of LAV were significantly smaller than all 2D and 3D-derived LAV. With regard to the different methods employed for LAV assessment, the 3D LAP has the highest correlation with body weight for all phases of the LA cycle. The mean left atrial ejection fraction (LAEF) was approximately 50% with range of 24-76% in our population. The functional indices are method-dependent and

may not be used interchangeably; the only functional index that correlated with BW in our population was total LA emptying volume. The interobserver variability for all LAV measurements was acceptable.

The results of our study support the hypothesis that 3D echocardiography is a feasible, noninvasive method to measure LAV in a population of normal dogs. The utility of 3D echocardiography in cardiac dysfunction also merits further investigative process.

Quantitative Evaluation of Left Atrial Volume and Function by One-dimensional, Two-dimensional, and Three-dimensional Echocardiography in a Population of Normal Dogs

by
Nicole L. LeBlanc

A THESIS

submitted to

Oregon State University

in partial fulfillment of
the requirements for the
degree of

Master of Science

Presented August 12, 2014
Commencement June 2015

Master of Science thesis of Nicole L. LeBlanc presented on August 12, 2014.

APPROVED:

_____

Major Professor, representing Veterinary Science

_____

Dean of the College of Veterinary Medicine

_____

Dean of the Graduate School

I understand that my thesis will become part of the permanent collection of Oregon State University libraries. My signature below authorizes release of my thesis to any reader upon request.

_____

Nicole L. LeBlanc, Author

ACKNOWLEDGEMENTS

The authors wish to thank the OSU cardiology veterinary technicians, Mrs. Amy Berry and Mrs. Robyn Panico, for enduring patience during the image acquisition phase of the study. The authors express sincere appreciation to Dr. Deborah Keys for her statistical expertise. And lastly the authors are grateful to the many dogs and owners who graciously volunteered to participate in this study.

CONTRIBUTION OF AUTHORS

Dr. LeBlanc solicited study participants and organized intake of participants. Dr. LeBlanc primarily performed data collection, and Dr. Sisson designed the study. Drs. LeBlanc and Sisson performed data measurements. Drs. LeBlanc, Sisson, and Scollan assisted collectively in the interpretation of data. Dr. LeBlanc generated the thesis document, which was edited by Drs. Sisson and Scollan.

TABLE OF CONTENTS

Page

TABLE OF CONTENTS (Continued)

LIST OF FIGURES

Figure Page

LIST OF TABLES

Table Page

LIST OF ABBREVIATIONS

Abbreviations table:

American Society of Echocardiography	ASE
Area-length method	ALM
Body surface area	BSA
Body weight	BW
Computed tomography	CT
Heart rate	HR
Left atrium	LA
Left atrial ejection fraction	LAEF
Left apical	LAP
Left atrial volume	LAV
Left atrial volume during the conduit phase of the left atrial cycle	LAV_c
Left atrial volume during the reservoir phase of the left atrial cycle	LAV_r
Left atrial volume during the systolic phase of the left atrial cycle	LAV_s
Left ventricle	LV
Magnetic resonance imaging	MRI
Method of disks (modified Simpson's)	MOD
Mitral regurgitation	MR

Mitral valve	MV
Right parasternal long-axis view	RLA
Right parasternal short-axis view	RSA
Real time 3-dimensional echocardiography	RT3DE
Two-dimensional left apical derived left atrial volume, biplane area-length method	2D Biplane
Two-dimensional left apical derived left atrial volume, monoplane area length method	2D LAP ALM
Two-dimensional left apical derived left atrial volume, monoplane method of disks	2D LAP MOD
Three-dimensional left apical derived left atrial volume, biplane technique using volume from 4- and 2-chamber views	3D Biplane
Three-dimensional left apical derived left atrial volume	3D LAP
Three-dimensional right parasternal long axis derived left atrial volume	3D RLA

Chapter 1

Introduction

The left atrium (LA) has numerous functions in the heart and therefore accurate assessment of the LA plays a critical role in determining the presence and extent of heart disease. Left atrial size is particularly integral in determining the presence of underlying heart disease in the absence of obvious valvular, myocardial, or pericardial dysfunction. The LA has several notable functions, including active and passive components. Left atrial performance is often assessed conventionally by LA size at sequential time points in the LA cycle. There is strong evidence that LA size and performance have prognostic value in predicting patient outcomes, via risk stratification for atrial fibrillation and thromboembolic events, and incidence of heart failure.[1]

Left atrial anatomy

The LA chamber consists of 2 embryologically distinct compartments, known as the LA (body) and the left auricle. The LA body results from outgrowth of pulmonary veins and the left auricle is a remnant of the embryonic LA.[2] The LA body has an irregular shape that does not approximate any traditional geometric model.[3] The left auricle and right auricle are separate structures viewed externally, bisected by the pulmonic trunk on the cranial surface of the heart. The left auricle is a finger-like pouch, extending cranially and confluent with the LA body.[3] The left auricular volume is 15-20% of total LAV in normal dogs.[4] Muscular bands, known as pectinate muscles, are a distinguishing featured of the auricle and absent in the body of the LA.[3] Despite the fact

that LA body walls are smooth, their thickness is not uniform.[5] In cadaveric subjects, the trans-mural thickness of the dorsal LA wall ranged from 3.5 to 6.5 mm, the lateral wall ranged from 2.5-4.9 mm, the anterior wall ranged from 1.5 to 4.8 mm, and the posterior wall ranged from 2.5-5.3 mm.[5] The area of the LA near the MV annulus, pulmonary venous confluence, and caudal to the aorta can be exceptionally thin with an average thickness of 2 mm.[5] Internally, the LA and right atrial body are divided by an interatrial septum.[5] The outflow portion of the LA forms a complex, non-planar, saddle-shaped structure with the mitral valve (MV). Adding complexity, the left auricle is also more compliant than the LA body, which has been documented in various left auricular appendage clamping studies.[6-8] To the author's knowledge, the etiology of this difference compliance has not been elucidated.

The pulmonary veins empty into the inflow region of the LA on the dorsolateral and dorsomedial aspect in dogs, with a more complex anatomic arrangement compared to people.[9] There are 5-8 (average of 7) pulmonary veins draining the canine LA, however many of these vessels anastomose prior to entering the LA.[9,10] The junction of the pulmonary veins to the LA is referred to as the ostia (*ostia venarum pulmonalium*).[9] In general, there are 3 major ostia in the dog: the cranial left ostia consisting of the left cranial portion and left caudal portion of the left cranial lung lobe, the caudodorsal ostia consisting of the left caudal, accessory, and right caudal lung lobe veins, and the right ostia consisting of the right middle and right cranial lobar veins.[9] Variation of this anatomy includes fused or separate ostia for the left cranial lung lobe portions, as well as left and right caudal pulmonary veins (D. Sisson, personal communication). The accessory vein can also have a separate ostium (D. Sisson, personal communication).

Grossly the LA chamber begins at the pulmonary veno-atrial junction and ends at the AV junction (fibro-fatty tissue plane).[5] However exactly where pulmonary venous tissue begins, and the LA tissue ends, is imprecise. One group documented the histologic and immunocytohistologic presence of a myocardial sleeve extending 1-2 cm into the pulmonary veins from the LA.[10] The presence of myocardial tissue in the proximal pulmonary veins is associated dynamically with changing orifice size in the pulmonary veins.[11]

Left atrial function

The LA cardiac cycle is conventionally divided into three descriptive phases known as reservoir (*r*), conduit (*c*), and systolic (*s*) phases. During the reservoir phase, the LA accumulates pulmonary venous blood during ventricular systole when the MV is closed. When LA pressure exceeds LV pressure and the MV opens to begin passive ventricular filling, the conduit phase occurs as blood from the pulmonary veins is passively conducted through the LA into the LV. The final phase occurs when the LA actively contracts during atrial systole, ejecting 15-30% of diastolic blood into the LV.[12] These phases are important in assessing LA performance via left atrial ejection fraction (LAEF), which is calculated by subtracting the smallest LAV (*s* phase) from largest LAV (*r* phase), divided by the largest LAV and multiplying by 100 for conversion to a percentage. Other indices are routinely used to assess the overall functional capabilities of the LA. These include active and passive constituents, and are based on the phasic functions described above:

- LA expansion index =

$$\frac{(LAV_r - LAV_s)}{LAV_s} \times 100$$

- Total LA emptying volume =

$$(LAV_r - LAV_s)$$

- Total LA emptying fraction =

$$\frac{(LAV_r - LAV_s)}{LAV_r} \times 100$$

- Passive LA emptying volume =

$$(LAV_r - LAV_c)$$

- Passive LA emptying fraction =

$$\frac{(LAV_r - LAV_c)}{LAV_r} \times 100$$

- Active LA emptying volume =

$$(LAV_c - LAV_s)$$

- Active LA emptying fraction =

$$\frac{(LAV_c - LAV_s)}{LAV_c} \times 100$$

Left atrial pressure waveforms

Pressure waveforms reflect the pressure changes that take place within a chamber or vessel throughout the cardiac cycle; the LA pressure waveform generally has 3 positive deflections and 2 descents.[12] Classically, description of the waveform begins at end-diastole and is denoted by the *a* wave, marking the increase in atrial pressure associated with atrial systole. This is associated with the P-wave on the surface ECG. The *a* wave is followed by the negative deflection known as the *x* descent, as the atria relax to allow for venous blood to return. A second positive deflection, the *c* wave, may interrupt the *x* descent and is associated with upwards movement of the atrioventricular valves during ventricular systole. The *v* wave is the third positive deflection that marks rising atrial pressure associated with venous filling against closed atrioventricular valves. This is associated with the T-wave on the ECG.

The right atrial and LA waveform are identical with 2 notable exceptions: the LA waveform has slightly higher pressures than the right, and the V wave of the LA can be higher than the A wave due to posterior constraint by the pulmonary veins, whereas the RA can decompress easily by vena cavae. When atrial pressure exceeds ventricular pressure, the atrioventricular valves open to begin early rapid ventricular filling. This reduction in atrial pressure is termed the *y* descent. Passive ventricular filling is followed chronologically by atrial diastasis where atrial pressure increases slightly but volume remains static. The end of diastolic is then again marked by active atrial contraction and the *a* wave. The LA pressure waveform is pictured:[13]

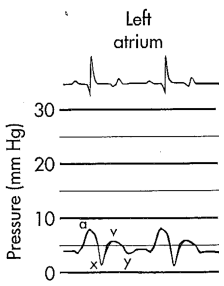

Left atrial pressure-volume curves

Normal LA function is depicted by the LA pressure-volume curves obtained from invasive cardiac catheterization.[14] This is the most accurate way to assess the mechanical function of the LA.[15] In the pressure-volume curves, 2 loops are formed: the A loop represents LA pump function and the V loop corresponds to left atrial reservoir function. The areas of both loops can be calculated and LA chamber stiffness derived as well.[16] In conditions such ventricular-based pacing or atrial fibrillation, loss of the A loop is noted. Physiologically the loss of atrial contraction is associated with a decrease in cardiac output of ~20%.[17]

Left atrial physiology

Like ventricular performance, a myriad of factors affect LA performance. An increase in either LA afterload or LA preload results initially in increased contractility, however atrial fiber length eventually reaches a threshold and function deteriorates subsequently.[18] This threshold reflects the Frank-Starling principle applied to the atrial muscle.[16] The principle objective of the ascending limb of the curve reflects an attempt to maintain normalized stroke volume.

The relationship between the LA and left ventricle (LV) is interdependent and dynamic. As LA size reflects LV pressures, the LA becomes an important barometer of LV diastolic burden. During ventricular diastole, the LA is exposed to LV pressures with MV opening. With increased LV filling pressure, LA pressures must rise to maintain LV

filling.[19] Increased wall tension results in structural changes in the atrial myocytes, physically manifest as atrial dilation.[19] LA remodeling is a complex process that is mediated in part by neuroendocrine factors such as atrial natriuretic peptide, brain natriuretic peptide, angiotensin II, and aldosterone.[20]

The relationship between increased LA size and increased LV filling pressures in the presence or absence of MV disease has been described.[21,22] LA preload increases with mitral regurgitation (MR) and with chronic MR, LA size and mass enlarge with initially enhanced atrial contractile function.[16,23] LA afterload most often increases with rising LV filling pressures secondary to diastolic dysfunction, making LA afterload reflective largely of downstream pressure.[16] Another pathologic increase in LA afterload occurs with mitral stenosis, where resistance to forward blood flow occurs secondary to a stenotic MV.

Therefore LA size often reflects broadly changes in pressure or volume, as a physiologic attempt to normalize increased wall stress. One example of the changing mechanics of the LA frequented cited are those evidenced in studies of human athletes. Trained athletes manifest increased LV chamber size, wall thickness, LV mass, and larger LV stroke volumes.[24] The increased stroke volume is correlated to increased passive and contracting LA volumes, although LAEF is not different between athletes and controls.[25] During exercise, LA reservoir and contractile properties are enhanced without changes in the conduit function.[25,26] The ability to redistribute LV filling and respond to hemodynamic changes is an important feature of the adaptive response. Again, the major limitation of active and passive volume-based assessment of the LA is that it does not discern easily between increased preload or enhanced function.

While LA contraction augments LV volume by ~20% in normal subjects, this percentage increases substantially with impaired LV relaxation.[1] Modulating factors for LA contractile force include intrinsic LA contractility, LV compliance, and LV end-diastolic pressure.[1] The most commonly cited example of increased LA contractility is age-related diastolic dysfunction resulting in enhanced atrial contraction. In people, an increase in atrial contraction corresponds to age-related increases in LV stiffness.[27] In this setting, LA conduit function is decreased and the reservoir function appears unchanged in association with age.[1] Other relevant examples of impaired diastolic filling that are associated with initially enhanced LA function include increased LV stiffness due to chronic systemic hypertension and hypertrophic cardiomyopathy, wherein the LA hypertrophies as a result of increased LA afterload.[16]

In predicting the risk for left-sided heart failure, LA size is crucial as there are very few conditions that result in left-sided congestion in the absence of LA enlargement (e.g. ruptured chordae tendinae causing an acute, massive increase in LA pressure). LA size in myocardial dysfunction and valvular disease is possibly the most important consideration for predicting likelihood and risk of heart failure. In dogs, the progression of valvular disease is variable with some rapidly declining to heart failure after a relatively brief asymptomatic phase, and others experience years without any clinical signs until they developed congestive signs.[28] Some affected dogs expire from other co-morbidities and never degenerate into heart failure. Several veterinary studies have identified LA size as an important indicator for identifying asymptomatic dogs at risk for the development of heart failure.[28-30]

Quantitative left atrial size and function

The LA can be assessed noninvasively by echocardiography, which is ideal in veterinary patients due to the relative affordability and lack of obligate heavy sedation or general anesthesia. The complexity of the LA mandates certain rules of measurement be applied since there are several LA features that make quantification problematic. The presence of pulmonary veins also creates a dilemma when it comes to measurement, as the boundaries of the ostia are indistinct and the proximal portions of the pulmonary veins are visualized with echocardiography in different imaging planes. The pulmonary veins are generally excluded from LA measurement at their ostia. Conventionally, instead of tracing along the dorsal surface of the MV, the base of the LA is formed by connecting a straight line from the MV annular ring. With few exceptions, the left auricle is generally excluded from measurement, however where the auricular orifice begins and the LA body ends is not well delineated echocardiographically.

Standard LA imaging planes have been described for echocardiography in many animal species.[31] Left atrial size can be assessed using linear dimensions (i.e. diameter), circumferential tracings, area measurements, and volume calculations.[32] Most often, 1-dimensional (1D) (also known as linear M-mode) and later 2-dimensional (2D) imaging have been used in veterinary studies to quantify LA size, most often utilizing single plane diameter measurements. M-mode has the advantage of high sampling frequency rates (1000 to 5000 pulses per second) compared to the slower sampling rate of 2D imaging (50 to 250 pulses per second), giving M-mode the relative advantage of improved temporal resolution specifically useful for interrogating rapidly moving cardiac structures. Two-dimensional echocardiography was developed in the 1970's to address

limitations associated with unidimensional M-mode, using initially a mechanical sector scanner that was eventually replaced by phased array technology to allow for real-time tomographic images. Two-dimensional imaging not only improved diagnostic capabilities, it also advanced M-mode capabilities with 2D guidance.[33]

During the last decade, 3D echocardiography has become commercially available to the practicing cardiologist. Three-dimensional echocardiography can conceptually be divided into 2 forms: the first involving offline reconstruction of 2D images that scan a single cross-sectional plane which are then digitally formatted into rectangular pixels; the second employs a matrix transducer with very densely packed piezoelectric elements to obtain a pyramidal image. The latter is referred to as real time 3-dimensional echocardiography (RT3DE). Matrix transducers have a significant increase in ultrasound elements (2,400-2,500) compared to 2D phased array probes (64-128 elements), which is largely possible due to recent advances in microelectrics.[34] In RT3DE, the US beam is moved through the scan volume electrically, rather by physical movement of the transducer.[35]

The modes most commonly used for RT3DE include live 3D, live 3D zoom, and full volume mode. Full volume mode is associated with wide angle (104° elevation, 104° longitudinal) pyramidal volumetric data acquisition to an entire cardiac chamber. One complete volumetric RT3DE data set is gathered from 4-7 cardiac subvolumes, each one provided from a single cardiac cycle, in full volume mode.[35] The rendering of subvolumes is associated with certain inherent challenges of RT3DE, such as stitching artifact that is present with respiratory-associated cardiac movement and changing R-R intervals (i.e. sinus arrhythmia). In contrast to full volume mode, live 3D has a relatively

narrow sector angle (30°elevation, 65°longitudinal).[35] However the narrower scan volume is associated with improved temporal and spatial resolution. This mode is particularly adept at visualizing smaller structures like cardiac valves, masses, or subtle vegetative lesions. Live 3D zoom is similar to 2D zoom function with user-defined cropping to focus on a specific region of interest. The major disadvantages of RT3DE involve the time necessary for offline analysis, the inferior image quality compared to 2D images due to poor resolution, and inability to reliably image arrhythmic patients.

Integral to the debate on LA size are questions regarding LA function. In addition to 1D, 2D, and 3D echocardiographic methods, there are several Doppler-derived indices that are helpful in assessing LA function. These include pulsed-wave Doppler, time velocity integration of trans-mitral flow, pulmonary venous flow, LA strain and strain rate, and speckle-tracking echocardiography.[18] While the Doppler methods are easily obtained, they are limited by dependency on both heart rate and loading conditions.[1] Pulmonary venous flow can also provide insight into phasic LA function with systolic, diastolic, and atrial reversal waves measured by pulsed-wave Doppler. An increase in atrial reversal wave velocity is thought to reflect increased LVEDP, as opposed to enhanced LA performance.[1] Tissue Doppler imaging has less load dependence though remains angle dependent, and intrinsic tethering of the myocardium to the MV and ventricular muscle makes differentiating isolated atrial motion challenging.[1] In contrast, speckle-derived strain and strain rate are independent of wall tethering and loading conditions.[1]

Relevant literature review

For several decades, echocardiographic assessment of LA size was based primarily on the maximal LA diameter on short-axis M-mode or 2D echocardiographic images. Measuring the LA by M-mode was initially performed in human medicine, where the measurement bisects the LA body.[36] While analogous linear M-mode measurements of the LA have been well described in dogs, concern exists that M-mode may result in transection of the left auricle rather than the body of the LA, resulting in underestimation of LA size in normal and diseased dogs since the left auricle may not accurately reflect changes in the LA body.[37,38]

Another issue apparent in the literature is the absence of standardization for LA measurement techniques. For example, some investigators used the leading edge verses trailing edge technique for M-mode measurements, some groups measured the internal dimensions of the LA, and others measured the plane of the LA in short-axis views only.[38-40] Some investigators required the pulmonic valve to be visualized requires an obliqued view, as opposed to being parallel with the MV annulus.[38-40] Study design was also variable with some investigators evaluating a single breed verses a large group of diverse breeds; others evaluated only normal dogs or were inclusive of a subpopulation of diseased animals.

One study evaluated 4 methods of 2D measurement (LA diameter in short axis, LA diameter in long axis, LA circumference in short axis, and LA cross-sectional area in short axis) in 36 dogs of various breeds and weights, ranging from 4 to 56 kg. Of note, the investigators used the internal edge technique and included the left auricle in the LA area measurement. The aorta was bisected by measuring from the non-coronary and right

coronary commissure to the far aortic wall, and LA diameter was measured in a line extending from the commissure between the non-coronary cusp and left-coronary cusps of the aortic valve.[39] Another study evaluated LA size in 166 dogs of a single breed (Cavalier King Charles Spaniels). Here the leading edge technique was used, and LA measured from the non-coronary and left coronary commissure to the opposite side of the LA wall.[38] Another group investigated 2D and 3D estimations of LA size in various breeds of dogs with and without heart disease. These investigators measured LA diameter in short-axis in a line bisecting the LA at the level of the interatrial fossa ovalis and parallel to the MV annulus.[40] This group included the left auricle in the LA area measurements and excluded it from all others.

Left atrial volume

Accurate measurement of the LA is notoriously problematic, given its irregular shape. Some physiologists have regarded the LA as a cylindrical-shaped structure. One study by Tsakairis et al. evaluating LA physiology in instrumented dogs with radio-opaque mitral annulus markers and angiography found that changes in atrial size were primarily related to eccentric changes in the anterioposterior axis, due to MV movement.[11] In contrast, the dorsal wall of the LA moved minimally. This study demonstrated the ability of the LA to change dimensions eccentrically in normal dogs.

Left atrial enlargement specifically can also be non-uniform in various planes including craniocaudal, mediolateral, and ventrodorsal directions.[41] In other words, measuring the LA in an anterior-posterior orientation only may not accurately represent LA size if enlargement has occurred primarily in a lateral fashion. The ability to enlarge eccentrically, combined with its complex geometry, reduces the sensitivity of a single LA

linear measurement in human medicine.[42] To address this issue, the measurement of additional 2D planes (i.e. biplane or triplane technique) increases the agreement between measured and actual LA size.[43]

Left atrial volume (LAV) is more accurate in assessing LA size, as large changes in volume may be reflected by small changes in linear measurements due to asymmetrical enlargement of the LA.[44] LAV can be measured or calculated in several different ways, which include echocardiography (1D, 2D, and 3D), computed tomography (CT), and magnetic resonance imaging (MRI).[21,45-47] Of the echocardiographic techniques, 1- and 2D LA measurements provide estimates of LAV using mathematical formulas with shape assumptions, whereas 3D echocardiography directly measures LAV. Furthermore, the major limitation of volume-derived LA parameters is the inability to distinguish between enhanced LA function secondary to increased preload compared to intrinsic improvements in LA compliance and contractility.[1]

As mentioned, each 1D- and 2D-based estimates of LAV requires geometric assumptions about LA shape. While the cube formula, derived from a linear LA dimension, is the simplest method for estimating LAV, this technique is considered inferior to more complex methods such as the MOD, ALM, and ellipsoid model.[42] The ellipsoid model assumes the LA is a prolate ellipse with 3 axes of measurement that are included in the equation:

$$\text{Ellipsoid chamber volume} = \left(\frac{4}{3}\pi\right)\left(\frac{L}{2}\right)\left(\frac{D_1}{2}\right)\left(\frac{D_2}{2}\right)$$

where L is the long axis dimension, D_1 and D_2 are orthogonal short axis dimensions. Clinically the long axis dimension (L) is obtained from the LAP 4C view, the anterior

posterior dimension from the RLA view (D_1), and the mediolateral dimension from the RSA view (D_2). The major advantage of this model is the absence of endocardial tracing, nonetheless it does underestimate LAV as any error in measurement of the 3 planes is less forgivable mathematically than a slightly stray point on LA planimetry.[48]

The ASE recommends quantification of LAV by the MOD (Simpson's rule) or biplane ALM from the LAP 4- and 2-chamber views.[42] LAV is then indexed to human BSA as BSA minimizes gender differences and obesity-related changes in LAV.[19] This improves the clinical utility of LA measurements for the assessment of individuals with substantial differences in body size.[49]

$$\mathrm{LAV_{ind}} = \frac{\mathrm{LAV\ (mL)}}{\mathrm{BSA\ (m^2)}}$$

The MOD states that the volume of a chamber is the sum of the subvolumes occupying that shape. In this algorithm the chamber is divided into a series of oval disks, each with height (h) and axis (D_1), and the ventral LA border being defined by the MV annulus. Single plane MOD uses the equation:

$$\text{Single plane MOD chamber volume} = \frac{\pi}{4}(\mathrm{h})\Sigma(\mathrm{D_1})^2$$

The single plane MOD assumes 4- and 2-chamber widths are identical (D_1=D_2), therefore the biplane MOD is preferred according to the ASE. The equation for the biplane MOD is expanded to include the orthoganol axis D_2:

$$\text{Biplane MOD chamber volume} = \frac{\pi}{4}(\mathrm{h})\Sigma(\mathrm{D_1})(\mathrm{D_2})$$

Lastly the single plane ALM planimeters the entire LA, thus obtaining an area (A_1) and a length (L) from the mitral annulus to the posterior wall in a 4-chamber LAP view. The single plane ALM assumes that $A_1=A_2$.

$$\textit{S}\text{ingle plane ALM chamber volume} = \frac{8(A_1)^2}{3\pi L}$$

The biplane ALM incorporates the orthogonal 2-chamber view, deriving a second area (A_2) and either taking the average or lesser of the 2 lengths. Both biplane ALM and MOD are recommended over single plane equations to reduce inaccuracies.[42] Regardless of the method used, there is relatively good agreement between these models in large scale human studies. The median normal LAV/BSA using the ellipse formula is 21 mL/m^2 in women and 22 mL/m^2 in men.[49] Using the biplane MOD the mean values reported for humans is 20 +/- 6 mL/m^2.[50] The single plane ALM mean LAV for normal people is 21+/-7 mL/m^2.

Regardless of the technique used, 2D-derived LAV tend to underestimate actual LAV compared to CT or MRI.[45,51] This 2D underestimation may increase as the LA enlarges.[52] RT3DE may increase the accuracy of cardiac chamber assessment, since RT3DE LAV is not based on geometric shape assumptions compared to 2D methods. One study comparing LAV obtained from 320 slice-CT with transthoracic 2D and 3D LAV found that all imaging modes were strongly positively correlated.[46] However the absolute value of LAV by CT was significantly greater than 2D or 3D measurements ($P<0.01$). The maximum LAV (mean±SD) for CT was 102.4±39.2 mL, for 3D was 53.6±21.1 mL, and 2D was 60.3±24.6 mL. The minimum LAV for CT was 79.3±41.7 mL, for 3D was 38.2±17.6 mL, and 2D was 41.2±20.8 mL. Another study with the same

comparative premises (except using a 64-slice multidetector CT) in people with normal or enlarged atria found much closer aligned absolute values, with the mean LAV 32.2±7.6 mL/m^2 by CT, 29.7±7.5 mL/m^2 by RT3DE, and 26.2± 5.8 mL/m^2 by 2D methods using the biplane ALM.[53] In this study, LAV by RT3DE correlated well with CT-derived LAV (r=0.95) with an 8% underestimation, and LAV by 2D echocardiography correlated less well with CT (r=0.86) with a 19% underestimation.

Overall, studies in human subjects indicate that RT3DE-derived LAV determinations agree closely with the volumes measured by MRI (regarded as the gold standard). However, RT3DE measures do tend to systematically underestimate LAV by approximately 8-24%.[45,52,53] In general, 3D-derived LAV are more closely correlated with MRI than 2D-derived LAV, although systematic underestimation of LAV is present in both 2D and 3D echocardiography.[41,54,55] This systematic bias may be due to several factors, including limited spatial resolution of echocardiography compared to MRI, dropout from the interatrial septum, errors in MV boundary, foreshortening or loss of lateral resolution on the LAP view.[51]

There is no consensus about which techniques are preferable for LAV quantification in dogs. Reference values for LAV, estimated by 2D echocardiography, have been published based on the study of a large cohort of dogs (n=237) of various breeds (12 breeds), sizes, and ages. A strong positive association was found between LAV and BW, with the upper 95th percentile of LAV=0.92 mL/kg. Interestingly a strong positive correlation was also found between LAV and breed type. Another study comparing M-mode to 2D echocardiography in normal dogs and those with mitral regurgitation (MR) found that linear M-mode measurements of the LA were significantly

smaller than the corresponding 2D values for both groups.[38] Conventional M-mode measurements were obtained in RSA at the aortic valve with 2D guidance, and 2D obtained in the same plane taking the transverse aortic and left atrial body dimensions.[38] When these 2D and M-mode values were indexed to aortic diameter (LA:Ao), there were no significant differences in the control group between M-mode and 2D indices. However in dogs with MR, the indexed 2D values were significantly greater, prompting the authors to suggest the 2D LA:Ao index is a more sensitive indicator of enlargement patterns than M-mode derived measures. This observation is probably due to the fact that 2D measurements are performed in region of the LA that more consistently indicative of overall LA size in comparison to the M-mode measures. Interestingly, this group found only a weak correlation between M-mode and 2D LA dimensions and BW.

RT3DE imaging has only recently been used to evaluate veterinary patients and the existing body of veterinary literature devoted to this topic is sparse. One group compared 1-, 2-, and 3D methods of LV volume assessment with cardiac MRI, concluding that RT3DE significantly underestimated LV volumes compared to cardiac MRI.[56] This group found that 1D calculations of LV volume overestimated, and 2D MOD and RT3DE underestimated, LV volume compared to cMRI. Excellent correlation with cMRI was found with real-time triplane echocardiography using the 3D probe. Another echocardiographic study compared several 2D methods against BW-indexed RT3DE maximum LAV in a population of normal and diseased dogs to find poor correlation between the 2 modalities in the absence of allometric scaling equations.[40] The best correlation was found between the RT3DE and the diameter of the LA in long axis with

$Y=aM^b$ where *Y* equaled the RT3DE-derived LAV, M was the 2D based measurement, and *a* and *b* were constants.

While the debate continues in veterinary and human medical circles regarding the absolute accuracy of RT3DE, a more fundamental issue is identification of an accurate and reproducible method of quantification, for which there is general consensus. In other words, RT3DE may ultimately prove to be more robust and less variable than currently employed 2D methods. Therefore the principal objective of this study was investigation of systematic differences of LAV using 1-, 2- and 3D echocardiography in a population of healthy dogs. We also sought to compare methods for interobserver variability to determine reproducibility. The last goal was to characterize functional indices using these methods in our population. We hypothesized that RT3DE measurements obtained from the LAP window would estimate LAV in an accurate and efficient manner with acceptable interobserver variability. We also hypothesized that M-mode derived measurements would significantly underestimate LAV.

Body mass indexing

Dividing an obtained measurement by body size is commonly employed in analyzing data. Indexing methods attempt to normalize one or more sources of variation; some factors that influence cardiac measurements in people include age, sex, race, athletic conditioning, and body size; the sex differences that exist are nearly entirely accounted for by gender-specific differences in overall body size.[49,50,57] With the exceptions of age, similar findings have been observed in the dog.[58-60] The use of BSA as a surrogate for BW is thought to be an improved estimation of physiologic processes. In other words, BSA correlates with metabolic rate functions such as oxygen consumption

where cardiac output is a function of the body's oxygen consumption. BSA is not measured directly in people, although height and weight measurements are accounted for in commonly used formulas:

$$BSA\ (\mathrm{m}^2) = 0.007184 \times \mathrm{weight}^{0.425}(\mathrm{kg}) \times \mathrm{height}^{0.725}(\mathrm{cm})$$

The ASE recommends using BSA when indexing echocardiographic measurements in people.

To complicate the issue further, there some supporting evidence that the basic BSA equation is inaccurate.[61] This equation is based upon the late 19th century observation that surface area and the geometric volume are related by a surface area equaling volume$^{(2/3)}$.[62] Though mammals are not geometrically similar, by convention the same equation is applied. The length of a cube is obtained by taking the cube root of its volume. The surface area of the cube is obtained by volume$^{2/3}$. The ratio of volume to mass remains constant with geometrically similar objects and dogs are conventionally treated as geometrically similar objects. Regardless of species, BSA is an exponential of BW expressed as K(BW)^{a} where K is the shape constant for a given species. K values vary not only in different species, but also amongst breeds of the same species.[61] Some also suggest that the traditional mass exponent (a = 2/3) may also be a source of inaccuracy, as one group found the mass exponent ranged from 0.41 and 1.04 in rodents, largely as a function of age.[63]

The principle of indexing measurements to a relatively static internal dimension is not uncommon in veterinary imaging; the well-known vertebral heart score is one example of this concept.[64] This measurement indexes the sum of the long and short axes of the heart against a vertebrae per heart sum. By convention, a right lateral radiograph is

used where the long axis of the heart is measured from the ventral border of the carina to the most ventral portion of the cardiac apex. The short axis is perpendicular to long axis measurements at the level of the caudal vena cava. These 2 measurements are summed and then compared against the number of thoracic vertebrae beginning at the fourth thoracic vertebrae. Vertebral malformations present a barrier to this measurement, which is particularly problematic in brachycephalic breeds who are predisposed to cardiac diseases.[65] In these dogs, vertebral heart scores may be useful for assessing progressive changes in cardiac size opposed to normality.

Reference intervals in general are problematic in dogs given diversity of the species, which encompasses wide variation in somatotypic conformation.[59] Significant breed differences have lead to the advent of breed-specific reference ranges to more accurately reflect normality within a breed.[59] While the original vertebral heart score concept was studied in 100 dogs of various breeds, subsequent studies have identified alternative breed-specific reference intervals for Beagles, Greyhounds, and Whippet dogs.[66-69] Furthermore a recent study of dogs with varying levels of degenerative valve disease indicated echocardiographic dimensions were normal in some dogs that had enlarged vertebral heart scores.[70] Perhaps the results of this study will prompt further investigations devoted to the establishment of breed-specific reference ranges.

Some veterinary cardiologists assume that a linear relationship exists between echocardiographic measurements and body size, but there is considerable debate surrounding this relationship. In both M-mode and 2D imaging, LA size is often indexed to the aortic diameter at the level of the aortic leaflets due to ease of imaging and the expectation that most cardiac diseases do not change aortic dimensions significantly,

making this ratio a relatively independent internal index.[38] It is hypothesized that aortic size better reflects body frame (osseous skeleton) than body weight.[39] Therefore a significant change in aortic dimension could potentially result in erroneously indexed LA size given this hypothesis. One veterinary study of 36 normal dogs found the aortic root diameter to be imperfectly correlated with BW in dogs.[39] This finding is difficult to explain, although variability of aortic measurement would decrease the agreement with BW. Alternatively linear dimensions may be more appropriately correlated with other linear dimensions of size (e.g. body length, approximated as $BW^{1/3}$), as opposed to volume (BW).

A large scale retrospective study of 494 dogs, ranging from 2.2–95 kg, found that the log-transformed M-mode variables were most closely related to an index of body length ($BW^{1/3}$), which was supportive of their stated hypothesis, substantiating the principles of dimensional consistency.[37] These authors suggest cardiac volumes should be linearly related to a volumetric measurement (like BW), cross-sectional areas relate linearly to BSA (proportional to $BW^{2/3}$), and linear cardiac dimensions relate to body length (proportional to $BW^{1/3}$). Another large study of 237 healthy dogs representing various breeds found a positive association (r^2=0.9-0.92) between LAV and BW using the ALM method, and that a common allometric exponent (0.67 or 1) did not differ significantly across breeds for LA function, which suggests there is no advantage to one over the other clinically.[71] This study also concluded that dogs of all sizes and breeds had a maximal LAV in the 95th percentile of 0.92 mL/kg. Another study evaluating LAV with RT3DE had a median of 0.6 (interquartile range 0.5-0.8) mL/kg for maximum LAV, and a minimum of 0.4 (interquartile range 0.3-0.5) for control dogs.[72]

Materials and methods:

Enrollment:

This study included prospective recruitment of dogs owned by persons affiliated with Oregon State University, College of Veterinary Medicine. To ensure appropriate variety of weight and breed, 40 dogs total were stratified into one of four groups (<10 kg, 10-25 kg, 25-40 kg, >40 kg). Dogs were initially considered for enrollment based on history, physical examination, and the absence of known co-morbid conditions (i.e. healthy animals with no known medical problems). Bloodwork was not routinely performed. All dogs were in sinus rhythm at the time of the study. When normal physical examination findings were coupled with unremarkable M-mode, 2D, and Doppler echocardiography, dogs were considered enrolled in the study.

This study was approved by the Institutional Animal Care and Use Committee at Oregon State University. Informed consent of the owner was obtained prior to study inclusion for each participant.

Echocardiography

Dogs were unsedated and lightly restrained in right and left lateral recumbency for the echocardiogram. All dogs underwent a comprehensive echocardiographic examination with a study protocol consisting of M-mode, 2D, Doppler (pulsed-wave and tissue Doppler imaging), and RT3DE imaging with continuous ECG monitoring. All examinations were performed by the same echocardiographer (NLL). The majority of 2D images were obtained with a 8-3MHz phased array transducer, and the remaining 2D images obtained with an X5-1 MHz matrix transducer. All RT3DE images were obtained

with an X5-1 MHz matrix transducer. All images were obtained on a Philips iE33 ultrasound unit (Philips Medical Systems, Andover, MA).

Phases of the left atrial cycle

For the reservoir phase, the frame with the largest end diastolic dimension prior to opening of the MV was used, corresponding to end ventricular systole. For the conduit phase, the frame directly before the beginning of the P-wave on the ECG was used (i.e. pre-atrial contraction). The minimal atrial volume was measured following atrial systole as the smallest LA frame occurring immediately after the P wave at MV closure.[19] Several functional indices were subsequently calculated using the formulas:

- LAEF = $$\frac{(LAV_r - LAV_s)}{LAV_r} \times 100$$
- LA expansion index = $$\frac{(LAV_r - LAV_s)}{LAV_s} \times 100$$
- Total LA emptying volume = $$(LAV_r - LAV_s)$$
- Total LA emptying fraction = $$\frac{(LAV_r - LAV_s)}{LAV_r} \times 100$$
    - NB: Same equation as LAEF
- Passive LA emptying volume = $$(LAV_r - LAV_c)$$

- Passive LA emptying fraction =

$$\frac{(LAV_r - LAV_c)}{LAV_r} \times 100$$

- Active LA emptying volume =

$$(LAV_c - LAV_s)$$

- Active LA emptying fraction =

$$\frac{(LAV_c - LAV_s)}{LAV_c} \times 100$$

M-mode echocardiography

The LA was measured in right parasternal short-axis (RSA) view at the level of the heart base according to conventional methods. The cursor was placed through the center of the aortic root and then continued through either the cranial portion of the LA or the caudal portion of the LA appendage. The measurements obtained from M-mode include the aortic diameter at end diastole and maximum LA diameter at the reservoir phase. The aorta was measured from the leading edge of the anterior aortic wall to the trailing edge of the posterior aortic wall in attempt to avoid the variable space between the aortic root and the LA according to current recommendations of the ASE (Figure 1).[42]

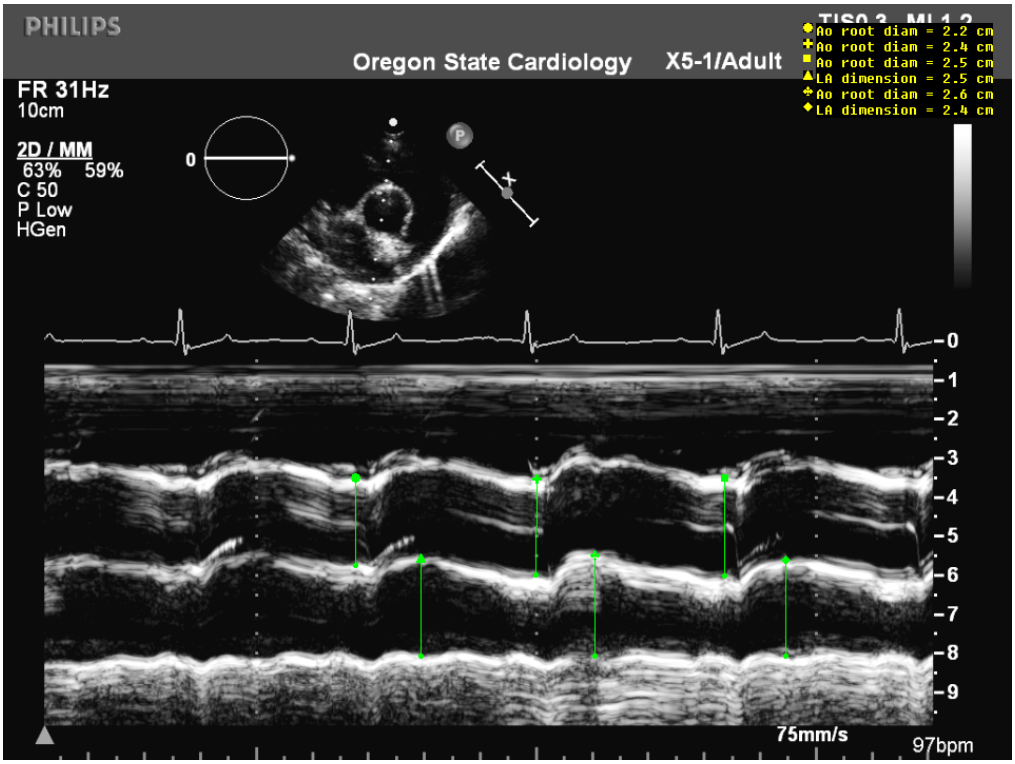

Figure 1: M-mode at the right parasternal short axis view

Figure 1 caption: M-mode at the level of the heart base in short axis.

The LA was measured from the leading edge of the medial LA wall to the leading edge of the lateral LA wall. Measurements were obtained over 3 consecutive beats and subsequently averaged. The average linear measurement was then entered into 2 equations for conversion of the linear measurement to a volumetric quantity.

$$\textit{S}\text{imple cube formula for LAV} = \text{D}^3$$

$$\text{Volume of a sphere formula} = \frac{4}{3}\pi\text{r}^3$$

where D equaled the LA diameter obtained from M-mode (as imaged above) and $\text{r} = \frac{D}{2}$.

2D echocardiography

For each included 2D imaging plane, a 5 beat loop was obtained, optimizing the LA. Both linear and volumetric measurements were performed for 3 consecutive beats and for the 3 distinctive phases of LA cycle. For the right parasternal short axis (RSA view), the LA was optimized and the chamber bisected. For both the right parasternal long axis (RLA) and LAP views, the LA was traced along the endocardial border, excluding the pulmonary veins and the LA appendage, to calculate LA circumference, area, and volume. To identify the ventral border of the LA, the hinge points of the MV were used. LA height was calculated from the center of the MV annulus line to the dorsal border of the LA (i.e. apicobasilar orientation). LA width was calculated at the widest portion of the LA, perpendicular to the LA height line, in a mediolateral orientation.

Single plane volume estimates were obtained from the RLA and LAP 4-chamber (4C) views using the MOD and area length (ALM) method. Biplane volume measurements were obtained using standard 4- and 2-chamber LAP images where the biplane ALM equation = $0.85\ [(A_1 \times A_2)/L]$; A_1 equals the LA area from the LAP 4C and A_2 equals the LA area from the LAP 2C view, and L is the average of the 2 lengths. For the MOD and ALM methods, planimetry was identical to that used for the biplane ALM, and automatic volume calculation was performed by a computer software package.

Sample images are provided.

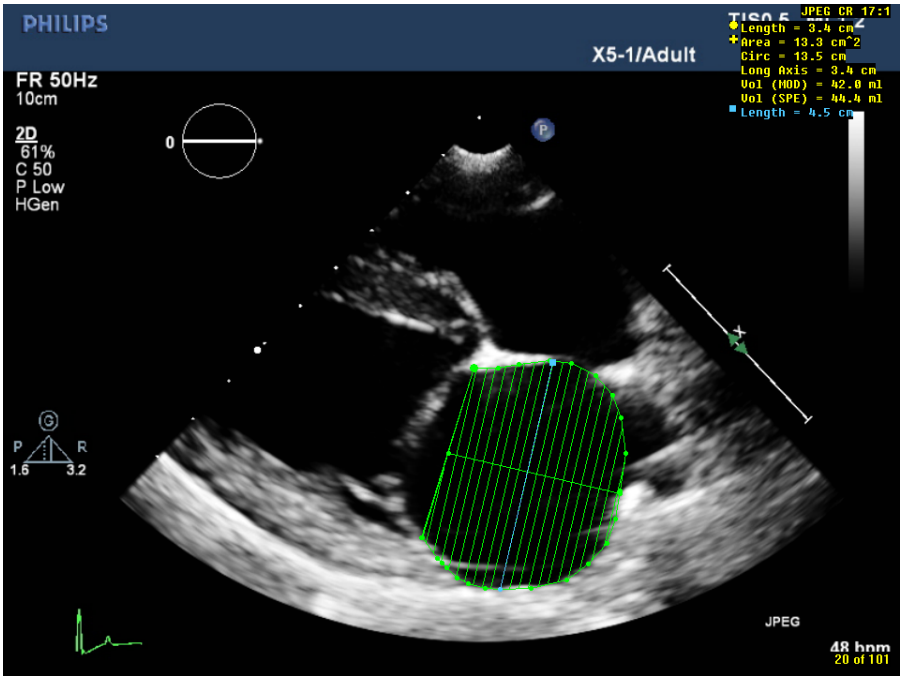

Figure 2: 2D right parasternal long axis image, reservoir phase

Figure 2 caption: right parasternal long axis image obtained during the reservoir phase.

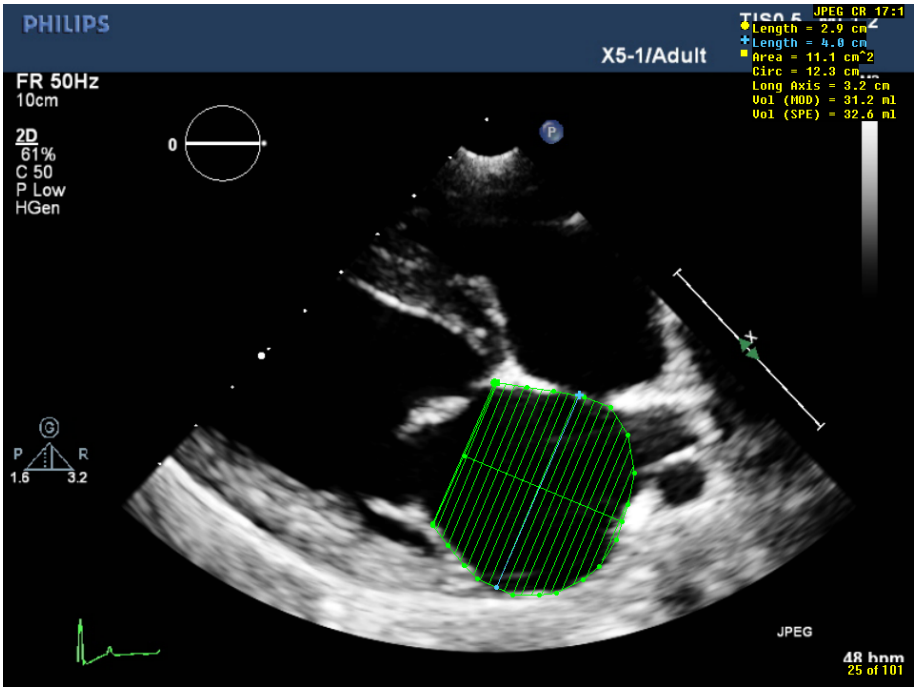

Figure 3: 2D right parasternal long axis image, conduit phase

Figure 3 caption: right parasternal long axis image obtained during the conduit phase.

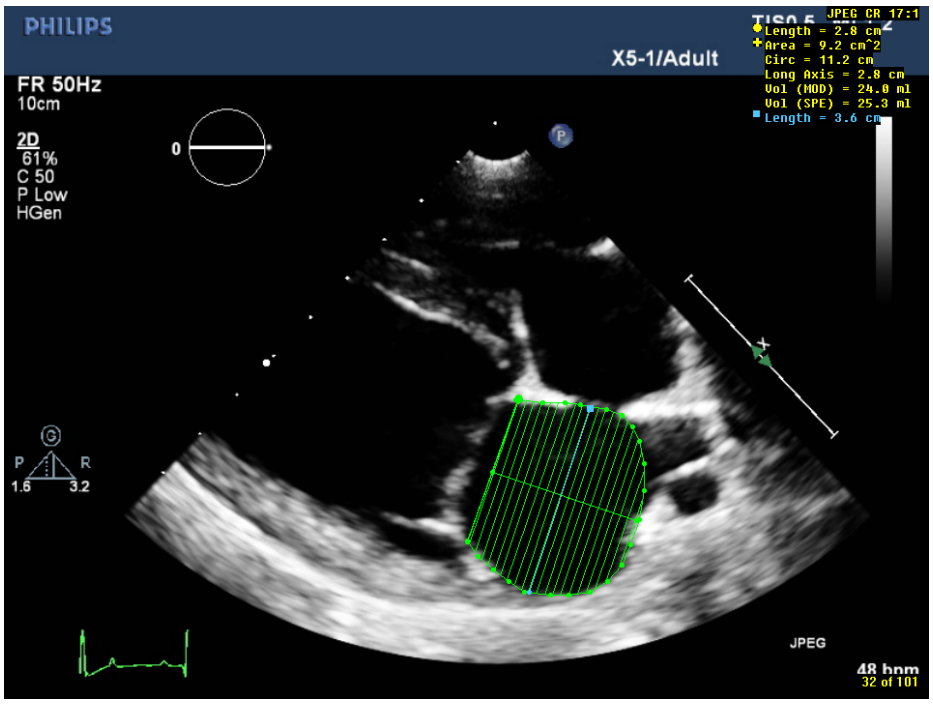

Figure 4: 2D right parasternal long axis image, systolic phase

Figure 4 caption: right parasternal long axis image obtained during the systolic phase.

On the RSA view, images were obtained at the level of the aortic valve with the aortic valve commissures visualized in ventricular diastole. The internal dimensions of the aorta and LA in short-axis were measured. The internal dimension of the LA body was also measured in a line extending from the commissure of non-coronary and left coronary aortic valve cusps to the distant margin of the LA. The aorta was measured in a conventional manner, bisecting the aorta from the commissure between the non-coronary and right coronary cusp to the opposite side. The aorta was also measured in a non-traditional fashion by bisecting the aorta between the non-coronary and left coronary aortic valve cusps.

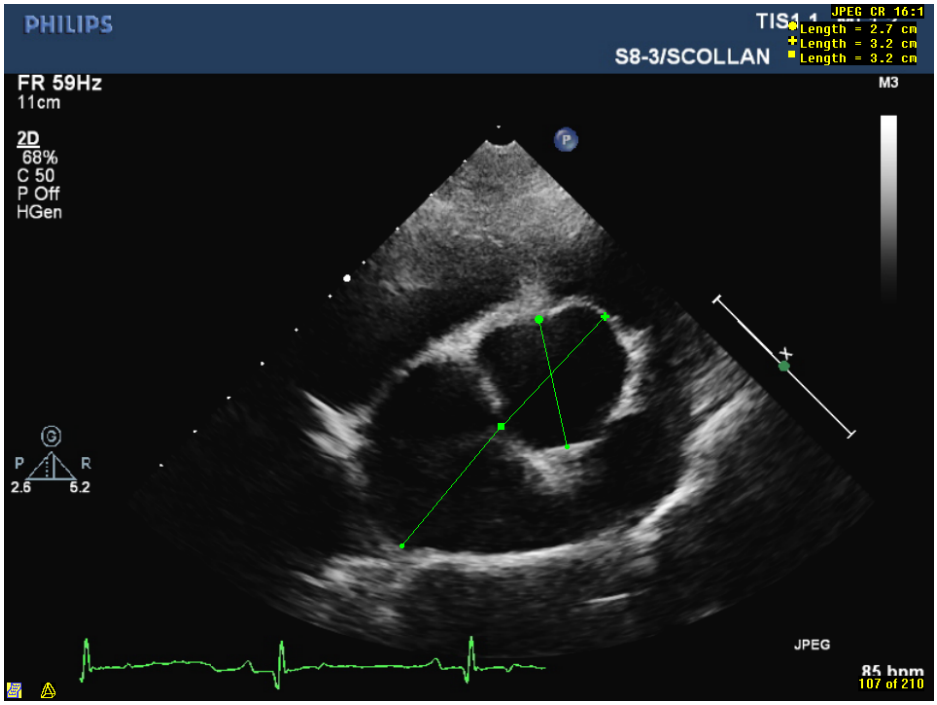

Figure 5: 2D right parasternal short axis image, reservoir phase

Figure 5 caption: right parasternal short axis image obtained during the reservoir phase.

In images where a pulmonary vein entered the LA in the desired measurement location, a curvilinear line was drawn between the visible margins of the LA. On some dogs, the dorsal portion of the LA on the LAP view had a protruding hyperechoic structure, which was confounding for measurement purposes (example figure 6).

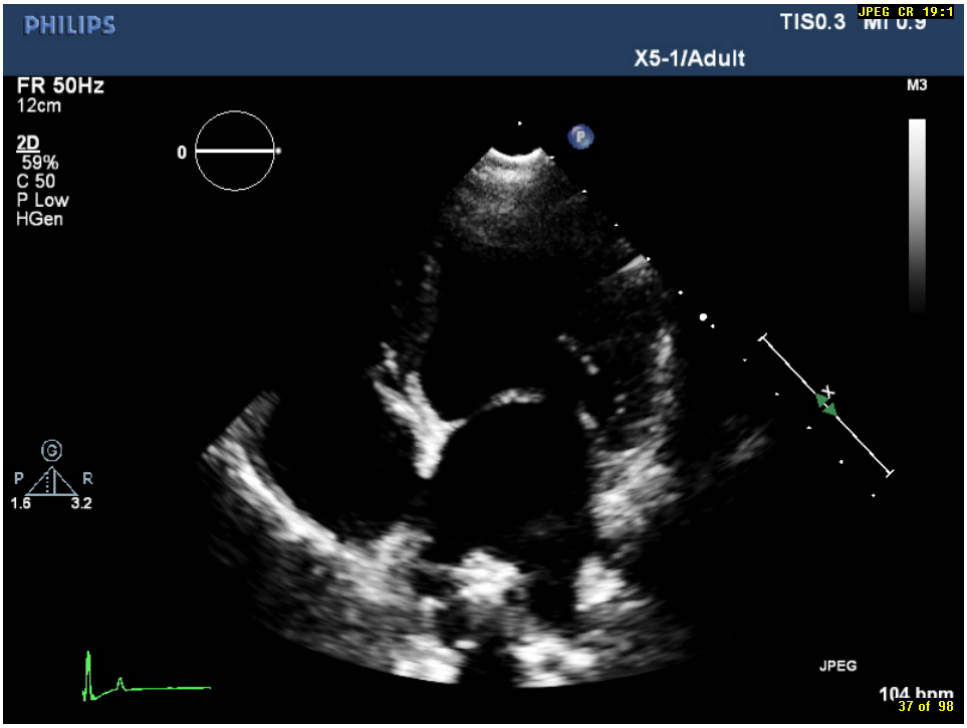

Figure 6: Left apical 4 chamber image

Figure 6 caption: left apical 4-chamber view depicting the hyperechoic dorsal left atrial wall.

In most cases, the dorsal wall was traced and this hyperechogenicity included in the lumen of the LA. This structure may be analogous to a ridge-like structure documented in normal humans between the left superior pulmonary vein and the left auricular os.[5] In people this ridge structure represents an infolding of the lateral atrial wall.[5] Other considered alternatives in this study include the ligament of Marshall, region of hyperechoic fat deposition, the confluence of right and left-sided pulmonary veins, or artifact.

3-D echocardiography

RT3DE volume images were acquired over 4 consecutive cardiac cycles to produce a complete data set in wide-angled full volume acquisition mode. Acquisition was triggered by appropriate recognition of the electrocardiographic R wave. The entire LA was carefully included in the 3D pyramidal data set, and 4 wedge-shaped subvolumes were obtained for each complete cardiac cycle. The images obtained were stored digitally and analyzed offline using Excelera, QLAB, and 3DQ-Advanced software programs (Philips Medical Systems, Andover, MA). Pyramidal data was displayed in 3 different planes (lateral, sagittal, and coronal) that were modified by manual shifting of horizontal and vertical lines.

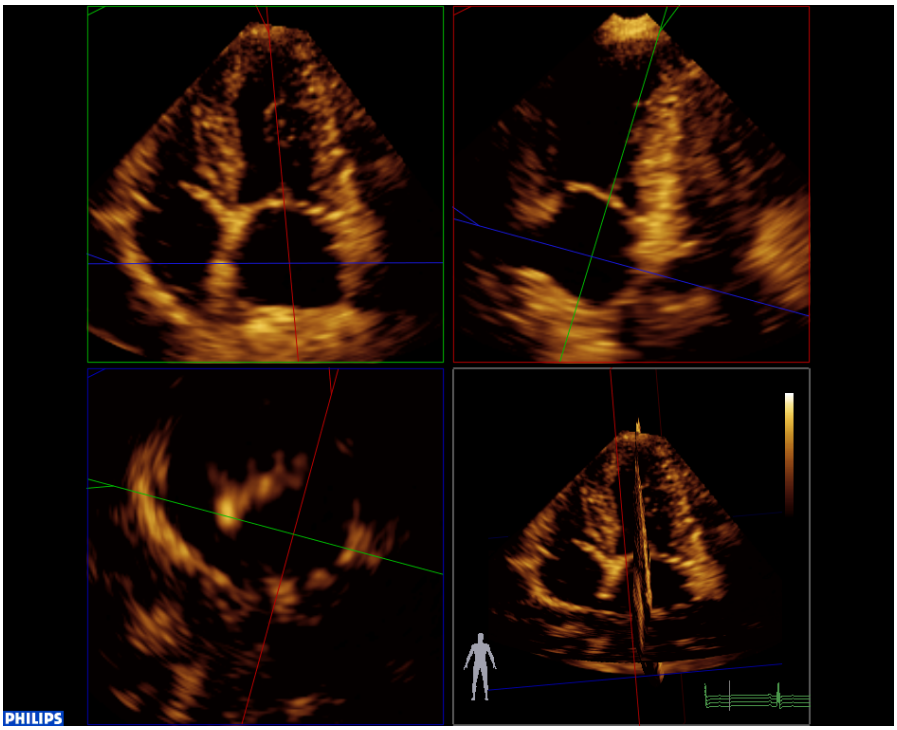

Figure 7: Post-processing display of 3D left apical images

Figure 7 caption: QLAB image displaying alignment of 3 imaging planes.

After the image was ideally aligned, offline analysis for 3D volume quantification involved manual identification of 5 anatomic reference points and a semi-automatically generated endocardial cast. One reference point was placed on the septal MV annulus and another point placed on the lateral MV annulus. The next 2 reference points were placed on the orthogonal image in an anterior and posterior orientation. The final reference point was placed at the dorsal border of the LA. The software program then automatically generated an endocardial cast of the LA using a deformable shell model. Manual adjustment along the endocardial border was subsequently performed in all examinations.

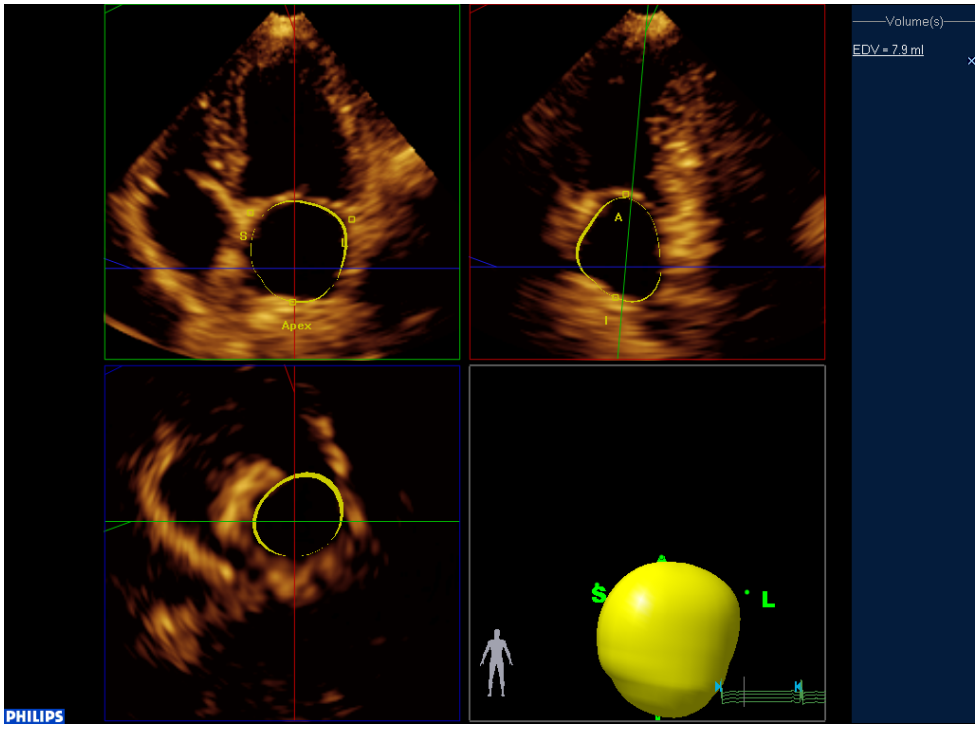

Figure 8: Sample of QLAB reservoir phase cast.

Figure 8 caption: QLAB image displaying reservoir phase endocardial image cast.

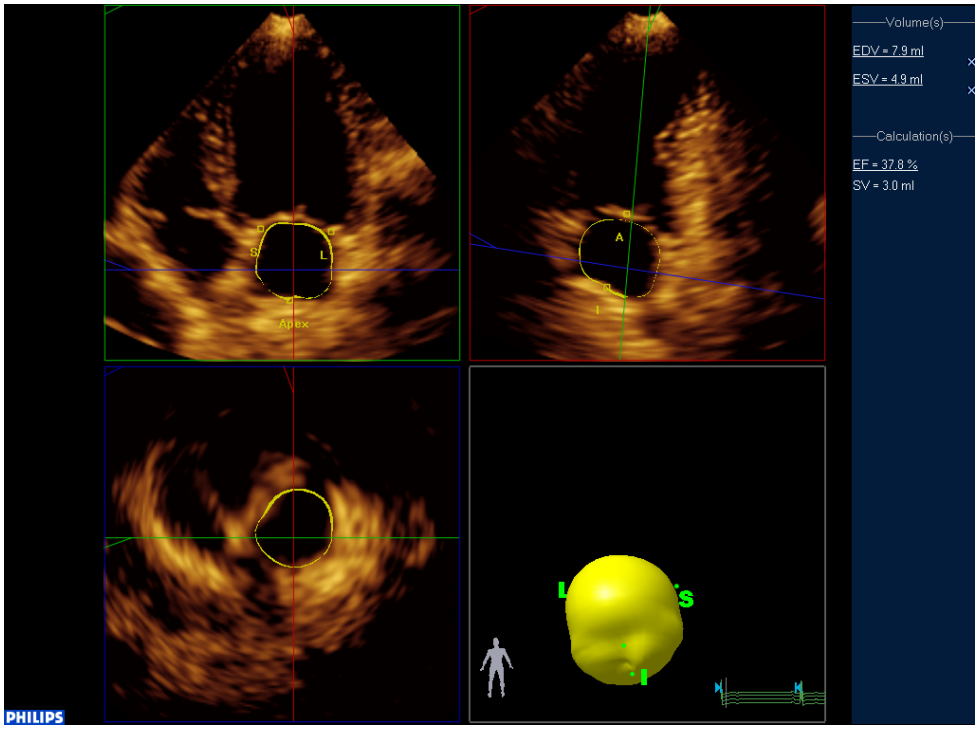

Figure 9: Sample of QLAB systolic phase cast

Figure 9 caption: QLAB image displaying systolic phase endocardial image cast.

Three individual beats were measured at the 3 previously described phases of the LA cycle using the previously described guidelines and subsequently averaged.

Evaluation of image quality:

One observer interpreted image quality for each 2D and 3D windows from the right and left imaging planes. Image quality was defined subjectively, stratifying images into excellent, acceptable, or marginal categories.

Variability analysis:

After completion of the initial phase of the study, a reproducibility study was performed to evaluate interobserver variability. One independent observer (DDS) repeated the

previously described measurements for 12 randomly selected dogs (3 per weight category), without knowledge of the results obtained by the initial observer (NLL).

Statistical analysis

Continuous variables are expressed as mean ±standard deviation (SD) and categorical data by their number (percentage). A repeated measures model that recognized multiple observations as belonging to the same dog was used to test for differences in quantification methods. The full model included a fixed factor of method and a random factor of dog. Multiple comparisons were adjusted for using Tukey's test. An unstructured covariance structure was used. All hypothesis tests were 2-sided and the significance threshold was set to 0.05.

Linear regressions were used to test for linear relationships between 1D, 2D, and 3D measurements of LAV dependent on BW or $BW^{0.75}$. Linear regressions were also used to test for linear relationships between functional indices and BW, as Goodness-of-fit was assessed by both coefficient of determination (r^2), a relative measure of model error ranging from 0 to 1 where higher is better, and root mean square error (root MSE), an absolute measure of model error which is in the same units as the dependent variable (volume in this case) where lower is better.

Least-squares regression analysis, performed on logarithmically transformed data, was used to develop power-law equations describing the relationship of LAV measurements to BW. Goodness-of-fit was assessed by coefficient of determination (r^2), a relative

measure of model error ranging from 0 to 1 where higher is better. Statistical analysis was performed using SAS version 9.2 (SAS Institute, Cary, NC, USA).

Interobserver variability analysis:

Mean, SD, and coefficient of variability (CV) of the 12 paired values were calculated, where the mean was the average of the 24 values and the SD was calculated as follows:

$$SD = \sqrt{\frac{\sum_{i=1}^{n}(x_1 - x_2)^2}{2n}}$$

where x_1 and x_2 are the paired values for i=1 to *n* pairs, and *n* equals the number of pairs (12 in this case). The coefficient of variability (CV) was calculated as the SD of the differences divided by the mean of the variable under consideration.

Results:

The study population included 40 dogs of various breeds including Golden retriever dogs (n=4), German Shepherd dogs (n=2), and one each of the following breeds: Yorkshire Terrier, Dachshund, Lhasa Apso, French Bulldog, Boston Terrier, Beagle, Standard Poodle, Greyhound, Borzoi, Great Pyrenees, Newfoundland, English Mastiff, and an Irish Wolfhound. The remaining 21 dogs were non-pedigreed dogs. Six additional dogs had been imaged and excluded based on poor image quality that precluded accurate tracing of the LA. There were 20 spayed females, 17 castrated males, 2 intact females and 1 intact male dog in the final group. The average age was 5.6 ± 2.8 years with a range 1.1 to 11.6 years. The average weight was 25 ± 17.7 kg with an overall range of 2 to 73 kg.

Tables 1-3 display descriptive statistics for reservoir, conduit, and systolic phases according to the 1D, 2D, and 3D methods used to calculate or measure LAV. All volumes are listed in milliliters (mL). M-mode values were obtained only for the reservoir phase of the cycle as the maximum left atrial size is conventionally measured.

Table 1: Descriptive statistics of LAV (reservoir phase)

Variable	**Mean**	**StdDev**	**Minimum**	**Maximum**
MM cube-r	9.533	7.565	1.214	29.791
MM sphere-r	4.992	3.961	0.635	15.599
2D RSA cube-r	24.123	19.102	2.370	87.130
2D RSA sphere-r	12.631	10.002	1.240	45.620
2D RLA MOD-r	30.915	24.017	2.200	86.967
2D RLA ALM-r	32.967	25.563	2.400	91.433
2D LAP MOD-r	27.028	20.155	2.000	89.100
2D LAP ALM-r	28.757	21.514	2.133	95.667
2D Biplane ALM-r	24.587	19.045	1.638	89.690
3D RLA-r	23.888	18.547	1.300	73.667
3D LAP-r	21.708	16.251	1.500	69.167
3D Biplane-r	21.993	16.357	1.487	61.200

Table 2: Descriptive statistics of LAV (conduit phase):

Variable	Mean	StdDev	Minimum	Maximum
2D RSA cube-c	19.062	15.728	2.032	64.00
2D RSA sphere-c	9.981	8.235	1.064	33.510
2D RLA MOD-c	23.823	19.549	1.9	70.833
2D RLA ALM-c	25.33	20.693	2.033	74.567
2D LAP MOD-c	21.731	17.451	1.767	69.9
2D LAP ALM-c	23.273	18.825	1.867	76.733
2D Biplane ALM-c	20.411	16.6	1.331	70.996
3D RLA-c	18.527	16.208	0.7	65.967
3D LAP-c	16.693	13.286	0.967	59.233
3D Biplane–c	17.279	13.922	0.897	52.847

Table 3: Descriptive statistics of LAV (systolic phase)

Variable	Mean	StdDev	Minimum	Maximum
2D RSA cube-s	11.777	10.552	1.147	42.875
2D RSA sphere-s	6.166	5.525	0.600	22.449
2D RLA MOD-s	15.961	14.006	0.833	52.833
2D RLA ALM-s	17.137	15.081	0.903	56.1
2D LAP MOD-s	14.108	12.191	0.797	52.6
2D LAP ALM-s	15.118	13.091	0.85	56.667
2D Biplane-s	13.478	11.669	0.59	51.85
3D RLA-s	12.921	11.559	0.533	48
3D LAP-s	12.272	10.197	0.5	46.567
3D Biplane-s	12.69	10.669	0.293	43.38

Significant differences between methods:

Histograms of the two data sets were compared with no major violations of normality assumptions and the significance threshold was set to 0.05. Table 4 displays the pairs of methods that were significantly different from eachother, along with the difference of the means (*e.g.*2D RLA MOD-r is significantly greater than 3D RLA-r, p=0.0004).

Table 4: List of significantly different paired method comparisons

METHOD A	METHOD B	Difference of Means A-B	Adjusted p-value
MM cube-r	2D Biplane-r	-15.1	<0.0001
MM cube-r	3D Biplane-r	-12.5	<0.0001
MM cube-r	3D LAP-r	-12.2	<0.0001
MM cube-r	3D RLA-r	-14.4	<0.0001
MM cube-r	2D LAP MOD-r	-17.5	<0.0001
MM cube-r	2D LAP ALM-r	-19.2	<0.0001
MM cube-r	2D RLA MOD-r	-21.4	<0.0001
MM cube-r	2D RLA ALM-r	-23.4	<0.0001
MM cube-r	2D RSA cube-r	-14.6	<0.0001
MM sphere-r	2D Biplane-r	-19.6	<0.0001
MM sphere-r	3D Biplane-r	-17.0	<0.0001
MM sphere-r	3D LAP-r	-16.7	<0.0001
MM sphere-r	3D RLA-r	-18.9	<0.0001
MM sphere-r	2D LAP MOD-r	-22.0	<0.0001
MM sphere-r	2D LAP ALM-r	-23.8	<0.0001
MM sphere-r	2D RLA MOD-r	-25.9	<0.0001
MM sphere-r	2D RLA ALM-r	-28.0	<0.0001
MM sphere-r	2D RSA cube-r	-19.1	<0.0001
MM sphere-r	2D RSA sphere-r	-7.6	0.0001
2D Biplane-c	2D RSA sphere-c	10.4	<0.0001
2D Biplane-r	2D RLA MOD-r	-6.3	0.0084
2D Biplane-r	2D RLA ALM-r	-8.4	<0.0001
2D Biplane-r	2D RSA sphere-r	12.0	<0.0001
2D Biplane-s	2D RSA sphere-s	7.3	0.0004
3D Biplane-c	2D LAP ALM-c	-6.0	0.0202
3D Biplane-c	2D RLA MOD-c	-6.5	0.0046
3D Biplane-c	2D RLA ALM-c	-8.1	<0.0001
3D Biplane-c	2D RSA sphere-c	7.3	0.0004
3D Biplane-r	2D LAP ALM-r	-6.8	0.0024
3D Biplane-r	2D RLA MOD-r	-8.9	<0.0001
3D Biplane-r	2D RLA ALM-r	-11.0	<0.0001
3D Biplane-r	2D RSA sphere-r	9.4	<0.0001
3D Biplane-s	2D RSA sphere-s	6.5	0.0048
3D LAP-c	2D LAP ALM-c	-6.6	0.0041
3D LAP-c	2D RLA MOD-c	-7.1	0.0008
3D LAP-c	2D RLA ALM-c	-8.6	<0.0001
3D LAP-c	2D RSA cube-c	6.7	0.0028
3D LAP-r	2D LAP ALM-r	-7.0	0.0010
3D LAP-r	2D RLA MOD-r	-9.2	<0.0001
3D LAP-r	2D RLA ALM-r	-11.3	<0.0001
3D LAP-r	2D RSA sphere-r	9.1	<0.0001
3D LAP-s	2D RSA sphere-s	6.1	0.0152

3D RLA-c	2D RLA ALM-c	-6.8	0.0021
3D RLA-c	2D RSA sphere-c	8.5	<0.0001
3D RLA-r	2D RLA MOD-r	-7.0	0.0011
3D RLA-r	2D RLA ALM-r	-9.1	<0.0001
3D RLA-r	2D RSA sphere-r	11.3	<0.0001
3D RLA-s	2D RSA sphere-s	6.8	0.0025
2D LAP MOD-c	2D RSA sphere-c	11.7	<0.0001
2D LAP MOD-r	2D RLA ALM-r	-5.9	0.0233
2D LAP MOD-r	2D RSA sphere-r	14.4	<0.0001
2D LAP MOD-s	2D RSA sphere-s	7.9	<0.0001
2D LAP ALM-c	2D RSA sphere-c	13.3	<0.0001
2D LAP ALM-r	2D RSA sphere-r	16.1	<0.0001
2D LAP ALM-s	2D RSA sphere-s	9.0	<0.0001
2D RLA MOD-c	2D RSA sphere-c	13.8	<0.0001
2D RLA MOD-r	2D RSA cube-r	6.8	0.0022
2D RLA MOD-r	2D RSA sphere-r	18.3	<0.0001
2D RLA MOD-s	2D RSA sphere-s	9.8	<0.0001
2D RLA ALM-c	2D RSA cube-c	6.3	0.0099
2D RLA ALM-c	2D RSA sphere-c	15.3	<0.0001
2D RLA ALM-r	2D RSA cube-r	8.8	<0.0001
2D RLA ALM-r	2D RSA sphere-r	20.3	<0.0001
2D RLA ALM-s	2D RSA sphere-s	11.0	<0.0001
2D RSA cube-c	2D RSA sphere-c	9.1	<0.0001
2D RSA cube-r	2D RSA sphere-r	11.5	<0.0001

M-mode derived LAV were significantly less than all 2D- and 3D-derived LAV methods for the reservoir phase. The 2D RLA MOD/ALM-r and 3D-derived RLA-r were significantly different, with the 2D values being greater than their 3D corollaries. The 2D-based RSA and RLA were also significantly different. The RSA-derived cube and spheric LAV were significantly different for all phases of the left atrial cycle, except the systolic phase. This indicates that the cube and sphere formulas are not interchangeable. The 2D RLA MOD-derived LAV were significantly greater than the RSA-derived spheric LAV during all phases of the cardiac cycle. The 2D LAP MOD-r was significantly less than 2D RLA MOD-r. The 2D LAP MOD/ALM were not significantly different than the RSA cube formula for any phase of the cycle. Importantly, 3D LAP

was not significantly different than the 2D LAP MOD or the 2D biplane for any phase of the cardiac cycle. To visualize the compared methods graphically, Bland-Altman plots were generated using GraphPad Prism 6.

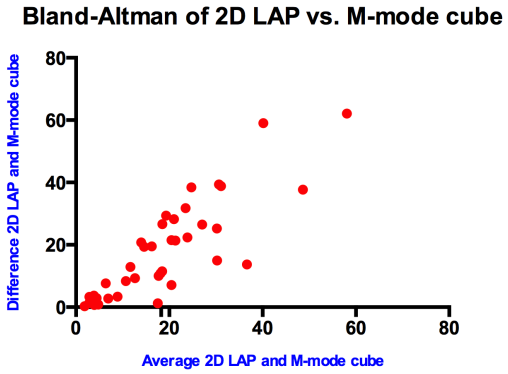

Figure 10: Bland-Altman comparing 2D LAP and M-mode cube

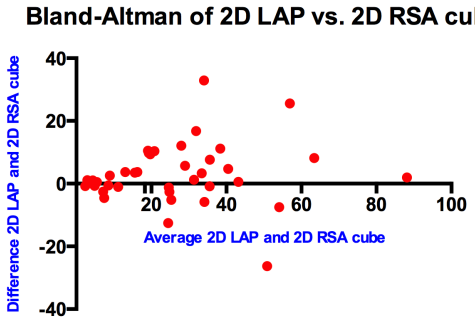

Figure 11: Bland-Altman comparing 2D LAP and 2D RSA cube formula

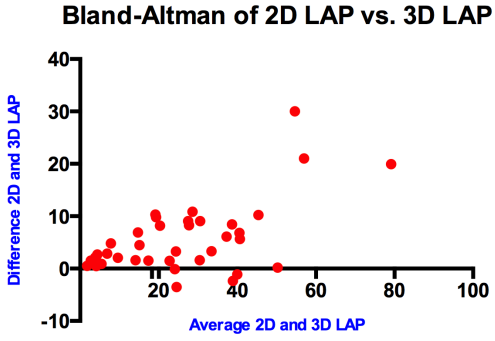

Figure 12: Bland Altman comparing 2D and 3D LAP

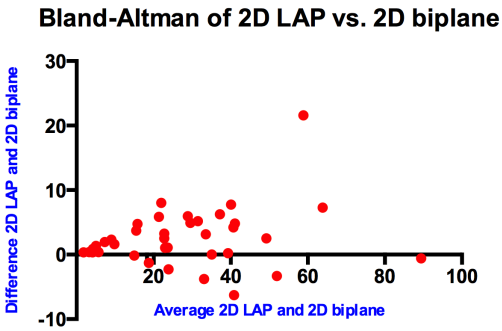

Figure 13: Bland-Altman comparing 2D LAP and 2D Biplane

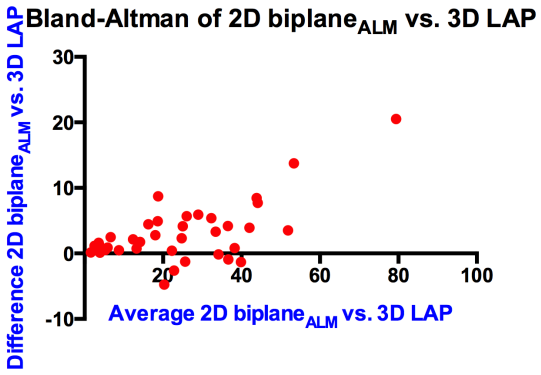

Figure 14: Bland-Altman comparing 2D Biplane and 3D LAP

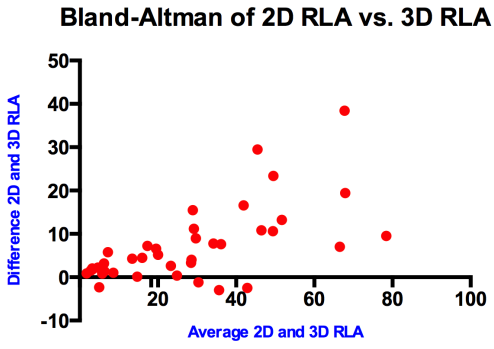

Figure 15: Bland-Altman comparing 2D and 3D RLA

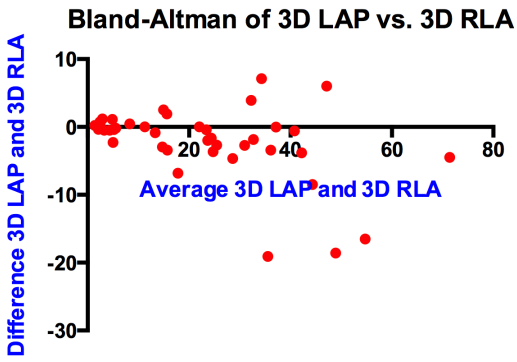

Figure 16: Bland-Altman comparing 3D LAP and 3D RLA

Linear regression analysis:

Based on our data, the relationship between LAV and BW or $BW^{0.75}$ varied depending on the method of estimation. Tables 5-7 display the goodness-of-fit statistics; both r^2 and root mean square error (MSE), for linear models of BW or $BW^{0.75}$ with reservoir, conduit, or systolic phases. The use of $BW^{0.75}$ was explored due to established allometric relationships identified when comparing the metabolic processes of animals of different species.[73] There appears to be a strong but imperfect linear relationship of 3D LAV with BW; the slight lack of agreement that does exist may be due to outliers present in the data set.

Table 5: Goodness-of-fit statistics of linear models of LAV (reservoir phase) and BW or $BW^{0.75}$

Variable	**r^2 (BW)**	**Root MSE (BW)**	**r^2 ($BW^{0.75}$)**	**Root MSE ($BW^{0.75}$)**
MM cube-r	0.4972	5.43	0.4987	5.43
MM sphere-r	0.4972	2.85[b]	0.4987	2.84[a]
2D RSA cube-r	0.7926	8.80	0.7698	9.3
2D RSA sphere-r	0.7926	4.60	0.7698	4.9
2D RLA MOD-r	0.8644	8.96	0.8589	9.14
2D RLA ALM-r	0.8661	9.48	0.8610	9.66
2D LAP MOD-r	0.7768	9.65	0.7804	9.57
2D LAP ALM-r	0.7808	10.21	0.7836	10.14
2D Biplane-r	0.8469	7.55	0.8348	7.84
3D RLA-r	0.8416	7.48	0.8427	7.45
3D LAP-r	0.8806[1]	5.69	0.8784[2]	5.74
3D Biplane-r	0.8104	7.21	0.8173	7.08

[1]Linear model with highest r^2.
[2]Linear model with 2nd highest r^2.
[a] Linear model with highest root mean square error.
[b] Linear model with 2nd lowest root mean square error.

Table 6: Goodness-of-fit statistics of linear models of LAV (conduit phase) and BW or $BW^{0.75}$

Variable	r^2 (BW)	Root MSE (BW)	r^2 ($BW^{0.75}$)	Root MSE ($BW^{0.75}$)
2D RSA cube-c	0.7581	7.80	0.7379	8.2
2D RSA sphere-c	0.7581	4.10[a]	0.7379	4.3[b]
2D RLA MOD-c	0.8256	8.27	0.8171	8.47
2D RLA ALM-c	0.8283	8.69	0.8202	8.89
2D LAP MOD-c	0.7777	8.34	0.7743	8.4
2D LAP ALM-c	0.7797	8.95	0.7748	9.05
2D Biplane-c	0.8448	6.62	0.8329	6.87
3D RLA-c	0.7992	7.36	0.7848	7.62
3D LAP-c	0.8582[1]	5.07	0.8504[2]	5.21
3D Biplane-c	0.7879	6.50	0.7884	6.49

[1]Linear model with highest r^2.
[2]Linear model with 2nd highest r^2.
[a]Linear model with highest root mean square error.
[b] Linear model with 2nd lowest root mean square error.

Table 7: Goodness-of-fit statistics of linear models of LA volume (systolic phase) and BW or $BW^{0.75}$

Variable	r^2 (BW)	Root MSE (BW)	r^2 ($BW^{0.75}$)	Root MSE ($BW^{0.75}$)
2D RSA cube-s	0.7776	5.0	0.7452	5.4
2D RSA sphere-s	0.7776	2.6[a]	0.7452	2.8[b]
2D RLA MOD-s	0.8408[2]	5.66	0.8256	5.93
2D RLA ALM-s	0.8303	6.29	0.8160	6.55
2D LAP MOD-s	0.7618	6.03	0.7533	6.13
2D LAP ALM-s	0.76	6.5	0.7518	6.61
2D Biplane-s	0.8216	5	0.8061	5.21
3D RLA-s	0.8013	5.22	0.7842	5.44
3D LAP-s	0.8497[1]	4.01	0.8366	4.18
3D Biplane-s	0.8066	4.75	0.802	4.81

[1]Linear model with highest r^2.
[2]Linear model with 2nd highest r^2.
[a]Linear model with highest root mean square error.
[b] Linear model with 2nd lowest root mean square error.

The results of the linear regression model indicate that 3D LAP measurements and BW had highest r^2 for reservoir, conduit, and systolic LAV. The root MSE was also very low for 3D LAP during all phases of the cardiac cycle. For reservoir LAV, the linear model of M-mode volume of sphere and $BW^{0.75}$ power had the lowest root MSE. This is because root MSE is an absolute measure of model error and M-mode measurements were much smaller absolute values, with smaller SD than any 2D or 3D volumes. The correlation between BW or $BW^{0.75}$ was also notably poor for M-mode. Also the RSA-sphere had moderate correlation with BW or $BW^{0.75}$ but had notably low MSE values. Select linear regressions are shown graphically below:

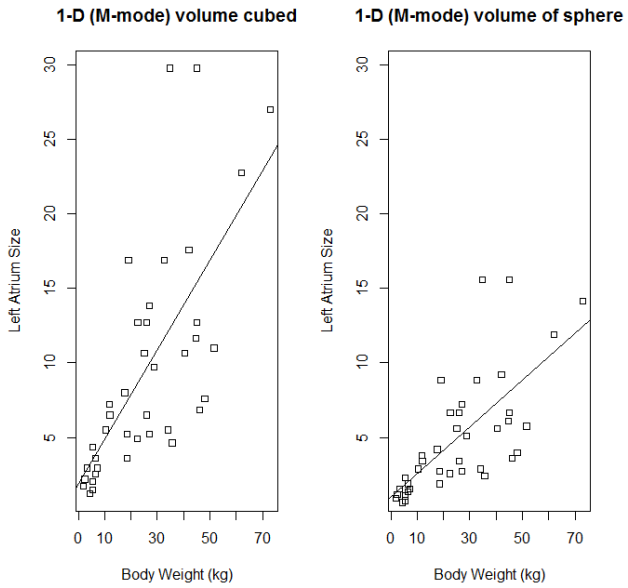

Figure 17: Linear regressions for M-mode-derived LAV compared to BW

Figure 17 caption: Linear relationships between M-mode derived LAV compared to BW.

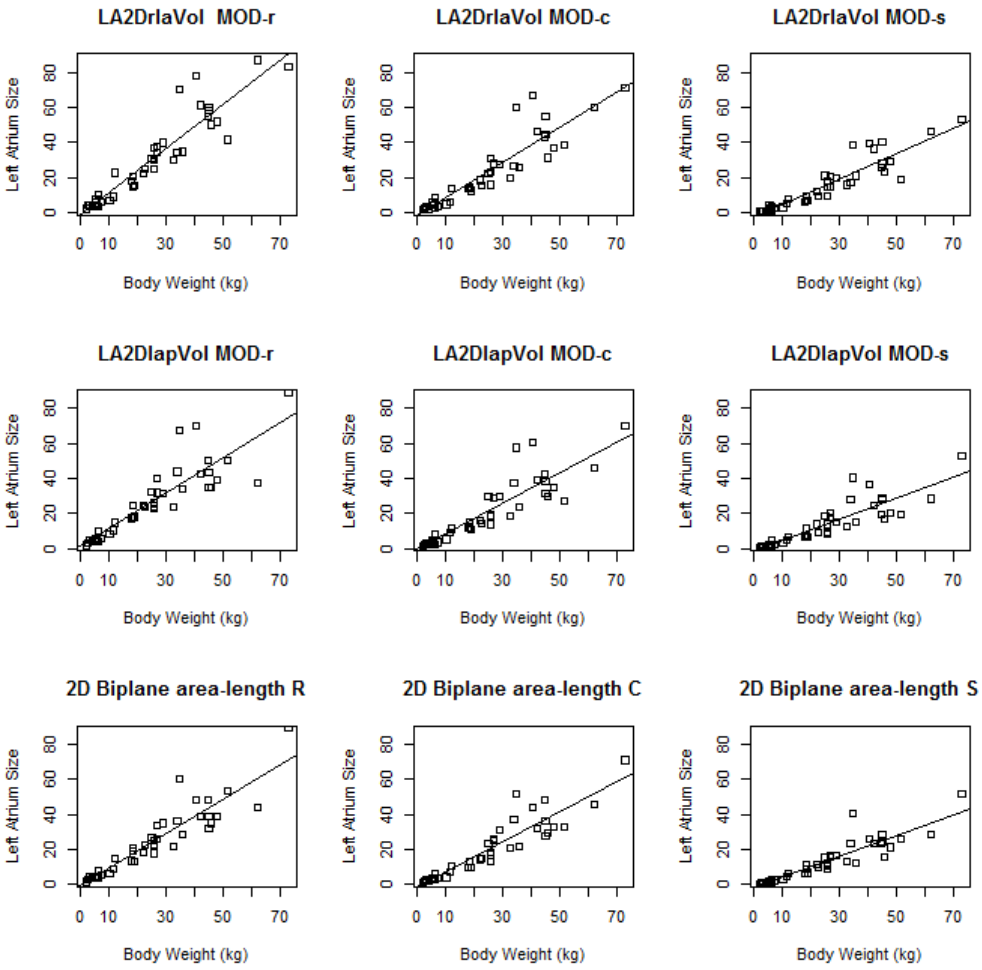

Figure 18: Linear regressions for 2D-derived LAV compared to BW

Figure 18 caption: Linear relationships between 2D-derived LAV compared to BW.

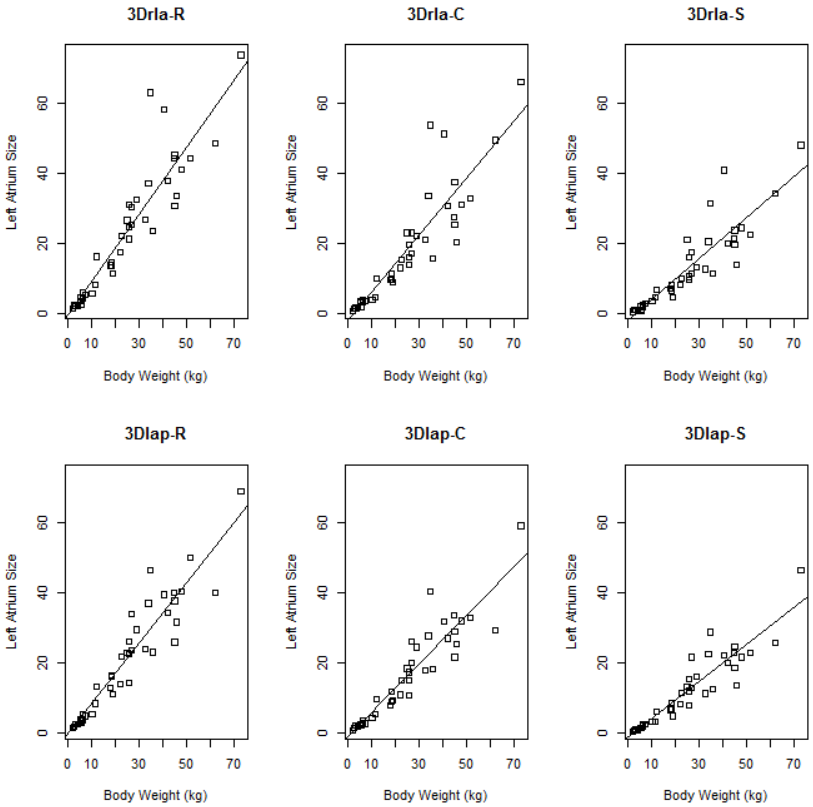

Figure 19: Linear regressions for 3D-derived LAV compared to BW

Figure 19 caption: Linear relationships between 3D-derived LAV to BW.

Regression equation:

Based on our linear regression analysis, the equations used to predict LAV for the 3 phases of the LA cycle using 2D LAP MOD are:

Phase	Predictive equation
r	LAV_{exp}=1.00231 * BW + 1.41185
c	LAV_{exp}=0.86838 * BW – 0.46289
s	LAV_{exp}=0.60038 * BW – 1.23607

The equations used to predict LAV for the 3 phases of the LA cycle using 3D LAP are:

Phase	Predictive equation

r	LAV_{exp}=0.86048 * BW – 0.28414
c	LAV_{exp}=0.69450 * BW – 1.0563
s	LAV_{exp}=0.53040 * BW – 1.28392

Despite the relatively robust linear relationship, we pursued nonlinear modeling as well. Table 8 displays the coefficients k and n for the fitted power-law relationship $LAV=k*BW^n$ and goodness-of-fit parameters.

Table 8: Coefficients and goodness-of-fits from power law fits

Variable	**n**	**k**	**r^2**
MM cube-r	0.73	0.84	0.6749
MM sphere-r	0.73	0.44	0.6749
2D Biplane-r	1.02	0.87	0.9399
2D Biplane-c	1.08	0.58	0.9308
2D Biplane-s	1.22	0.24	0.9451
3D Biplane-r	1.05	0.70	0.9352
3D Biplane-c	1.14	0.40	0.9292
3D Biplane-s	1.29	0.17	0.9308
3D LAP-r	1.08	0.63	0.9554
3D LAP-c	1.12	0.42	0.9532
3D LAP-s	1.20	0.23	0.9519
3D RLA-r	1.14	0.55	0.946
3D RLA-c	1.20	0.35	0.9408
3D RLA-s	1.26	0.19	0.9345
2D LAP MOD-c	1.03	0.73	0.9067
2D LAP MOD-r	0.98	1.10	0.9306
2D LAP MOD-s	1.17	0.28	0.9032
2D LAP ALM-c	1.03	0.77	0.9072
2D LAP ALM-r	0.98	1.15	0.9308
2D LAP ALM-s	1.18	0.30	0.9032
2D RLA MOD-c	1.09	0.65	0.9148
2D RLA MOD-r	1.06	0.95	0.9262
2D RLA MOD-s	1.25	0.25	0.9275
2D RLA ALM-c	1.08	0.71	0.914
2D RLA ALM-r	1.06	1.01	0.9232
2D RLA ALM-s	1.24	0.27	0.9252
2D RSA cube-c	0.93	0.90	0.8778

2D RSA sphere-c	0.93	0.47	0.8778
2D RSA cube-r	0.91	1.20	0.8884
2D RSA sphere-r	0.91	0.63	0.8884
2D RSA cube-s	0.95	0.49	0.8491
2D RSA sphere-s	0.95	0.26	0.8491

The derived exponent (BW^n) was ~1 in most cases, which supports a linear relationship between LAV and BW. In other words, if n=1 in the equation $LAV=k*BW^n$, then the equation functionally becomes LAV=k*BW, which is equivalent to a linear equation (y=mx+b) with a zero-intercept. This is similar to the equation used for allometric scaling $Y=aM^b$ with Y equaling chamber size (volume, area, or linear dimension), M equaling body weight, and *a* and *b* are constants. *A* is the proportionality constant, and *b* is the scaling exponent and the slope of the regression line. Using these principles, volume equals aM^1, surface area equals $aM^{2/3}$, and length equals $aM^{1/3}$.

Functional indices:

Table 9 displays the descriptive statistics for LAEF variables; data is listed in percentages.

Table 9: Descriptive statistics of LAEF variables

Variable	N	Mean	StdDev	Minimum	Maximum
2D RSA cube, sphere	40	52.531	11.966	25.814	72.672
2D RLA MOD EF	40	53.354	10.825	30.400	79.603
2D LAP MOD EF	40	53.020	12.803	20.913	78.151
2D biplane EF	40	50.262	11.786	24.210	76.320
3D RLA EF	40	50.018	10.771	21.330	71.196
3D LAP EF	40	47.396	8.988	27.692	66.667

The overall LAEF were similar between 2D and 3D methods, with an overall LAEF average of 50% ±10%. The LAEF was not performed on M-mode data since only one time point was obtained for this modality.

Table 10 displays the goodness-of-fit for the linear models of LAEF variables and BW or $BW^{0.75}$.

Table 10: Goodness-of-Fit Statistics of Linear Models of LAEF and $BW/BW^{0.75}$

Variable	r^2 (BW)	Root MSE (BW)	r^2 ($BW^{0.75}$)	Root MSE ($BW^{0.75}$)
2D RSA	0.0551	12.0	0.0468	12.1
2D RLA MOD LAEF	0.4002	8.49	0.4286[2]	8.29[b]
2D LAP MOD LAEF	0.4019	10.04	0.4134	9.93
2D Biplane LAEF	0.4249[3]	9.05	0.4616[1]	8.76
3D RLA LAEF	0.2622	9.37	0.2654	9.35
3D LAP LAEF	0.3771	7.19[b]	0.3993	7.06[a]

A strong correlation was not identified between BW or $BW^{0.75}$ in this population of dogs based on the results of the linear regression analysis presented in table 10.

Table 11 displays pairs of methods that were significantly different from eachother for functional indices, along with the difference of the means.

Table 11: Significantly different paired method comparisons for functional (fraction) indices

Variable	METHOD A	METHOD B	Difference of Means A-B	Adjusted p-value
LA expansion index	2D RLA MOD	3D LAP	32.2	0.0237
LA expansion index	2D RSA cube	3D LAP	31.2	0.0326
LA expansion index	2D RSA sphere	3D LAP	31.1	0.0325
LA expansion index	2D LAP MOD	3D LAP	34.6	0.0109
Total LA emptying fraction	2D RLA MOD	3D LAP	6.0	0.0257
Total LA emptying fraction	2D LAP MOD	3D LAP	5.6	0.0437
Active LA emptying fraction	2D RLA MOD	3D LAP	8.2	0.0365
Active LA emptying fraction	2D RSA cube	3D LAP	9.7	0.0067
Active LA emptying fraction	2D RSA sphere	3D LAP	9.8	0.0053

Active LA emptying fraction	2D LAP MOD	3D LAP	10.0	0.0044
Active LA emptying fraction	2D Biplane	3D LAP	8.2	0.0399

Table 12: Significantly different paired method comparisons for functional (volume) indices

Variable	**METHOD A**	**METHOD B**	**Difference of Means A-B**	**Adjusted p-value**
Total LA emptying volume	2D RLA MOD	2D RSA sphere	8.5	<0.0001
Total LA emptying volume	2D RLA MOD	2D Biplane	3.8	0.0006
Total LA emptying volume	2D RLA MOD	3D RLA	4.0	0.0003
Total LA emptying volume	2D RLA MOD	3D LAP	5.5	<0.0001
Total LA emptying volume	2D RSA cube	2D RSA sphere	6.1	<0.0001
Total LA emptying volume	2D RSA cube	3D LAP	3.1	0.0136
Total LA emptying volume	2D RSA sphere	2D LAP MOD	-6.5	<0.0001
Total LA emptying volume	2D RSA sphere	2D Biplane	-4.6	<0.0001
Total LA emptying volume	2D RSA sphere	3D RLA	-4.5	<0.0001
Total LA emptying volume	2D RSA sphere	3D LAP	-3.0	0.0201
Total LA emptying volume	2D LAP MOD	3D LAP	3.5	0.0029
Passive LA emptying volume	2D RLA MOD	2D RSA sphere	4.4	<0.0001
Passive LA emptying volume	2D RLA MOD	2D Biplane	2.9	0.0067
Passive LA emptying volume	2D RSA cube	2D RSA sphere	2.5	0.0341
Passive LA emptying volume	2D RSA sphere	2D LAP MOD	-2.6	0.0201
Passive LA emptying volume	2D RSA sphere	3D RLA	-2.7	0.0157
Active LA emptying volume	2D RLA MOD	2D RSA sphere	4.0	<0.0001
Active LA emptying volume	2D RLA MOD	3D RLA	2.3	0.0182
Active LA emptying volume	2D RLA MOD	3D LAP	3.4	<0.0001
Active LA emptying volume	2D RSA cube	2D RSA sphere	3.5	<0.0001
Active LA emptying volume	2D RSA cube	3D LAP	2.9	0.0006
Active LA emptying volume	2D RSA sphere	2D LAP MOD	-3.8	<0.0001
Active LA emptying volume	2D RSA sphere	2D Biplane	-3.1	0.0002
Active LA emptying volume	2D LAP MOD	3D LAP	3.2	0.0001
Active LA emptying volume	2D Biplane	3D LAP	2.5	0.0052

These results support dependency on the method employed. In other words, functional indices obtained by one method are not necessarily translational to another method. With the exception of the passive indices, the 2D and 3D LAP were significantly different.

We sought to explore the relationship between functional indices and $BW/BW^{0.75}$. Table 12 displays the goodness-of-fit statistics, both r^2 and root MSE for linear models of BW with 49 functional indices.

Table 13: Goodness-of-fit statistics of linear models of functional indices and BW

Variable	r^2	Root MSE
LA expansion index 2D RLA MOD	0.3573	53.3
Total LA emptying volume 2D RLA MOD	0.7876	5.0
Total LA emptying fraction 2D RLA MOD	0.4002	8.5
Passive LA emptying volume 2D RLA MOD	0.5966	3.8
Passive LA emptying fraction 2D RLA MOD	0.0402	10.6
Active LA emptying volume 2D RLA MOD	0.5662	4.4
Active LA emptying fraction 2D RLA MOD	0.2609	12.1
LA expansion index 2D RSA cube	0.0584	62.6
Total LA emptying volume 2D RSA cube	0.6321	6.0
Total LA emptying fraction 2D RSA cube	0.0551	12.0
Passive LA emptying volume 2D RSA cube	0.2867	5.3
Passive LA emptying fraction 2D RSA cube	0.0173	14.6
Active LA emptying volume 2D RSA cube	0.4853	4.6
Active LA emptying fraction 2D RSA cube	0.0420	16.2
LA expansion index 2D RSA sphere	0.0584	62.6
Total LA emptying volume 2D RSA sphere	0.6321	3.1
Total LA emptying fraction 2D RSA sphere	0.0551	12.0
Passive LA emptying volume 2D RSA sphere	0.2867	2.8
Passive LA emptying fraction 2D RSA sphere	0.0173	14.6
Active LA emptying volume 2D RSA sphere	0.4853	2.4
Active LA emptying fraction 2D RSA sphere	0.0420	16.2
LA expansion index 2D LAP MOD	0.3363	60.1
Total LA emptying volume 2D LAP MOD	0.6185	5.7
Total LA emptying fraction 2D LAP MOD	0.4019	10.0
Passive LA emptying volume 2D LAP MOD	0.1999	4.8
Passive LA emptying fraction 2D LAP MOD	0.1527	12.8
Active LA emptying volume 2D LAP MOD	0.5929	4.0
Active LA emptying fraction 2D LAP MOD	0.2285	11.2
LA expansion index 2D Biplane	0.3890	46.7
Total LA emptying volume 2D Biplane	0.7315	4.3
Total LA emptying fraction 2D Biplane	0.4249	9.1
Passive LA emptying volume 2D Biplane	0.2457	4.0
Passive LA emptying fraction 2D Biplane	0.1990	10.6
Active LA emptying volume 2D Biplane	0.6266	3.7
Active LA emptying fraction 2D Biplane	0.2119	11.2

LA expansion index 3D RLA	0.2685	40.6
Total LA emptying volume 3D RLA	0.7151	4.3
Total LA emptying fraction 3D RLA	0.2622	9.4
Passive LA emptying volume 3D RLA	0.3698	3.3
Passive LA emptying fraction 3D RLA	0.1338	11.1
Active LA emptying volume 3D RLA	0.6328	3.2
Active LA emptying fraction 3D RLA	0.0555	12.1
LA expansion index 3D LAP	0.3389	30.2
Total LA emptying volume 3D LAP	0.7950	3.0
Total LA emptying fraction 3D LAP	0.3771	7.2
Passive LA emptying volume 3D LAP	0.6626	2.1
Passive LA emptying fraction 3D LAP	0.1401	7.8
Active LA emptying volume 3D LAP	0.6224	2.3
Active LA emptying fraction 3D LAP	0.1598	10.1

These results suggest the total LA emptying volume is moderately correlated with BW for the measured/calculated LAV (2D/3D biplane, 2D/3D RLA, 2D/3D LAP, 2D RSA). The highest correlation with BW is LAV derived from 3D LAP (r^2=0.795). The fractional indices (passive, active, total emptying fractions) had no consistent relationship to BW. This finding is likely due to the fact that volume differences effectively become less relevant (i.e. cancel out) when divided by a denominator volume.

Interobserver variability:

Table 12 displays the SD, mean, and CV for the 12 paired of values obtained from the 2 observers. There were notable differences between the various methods. The variability noted in the 2D RSA-derived LAV was very high (>20%) for all phases of the left atrial cycle. The variability for M-mode- and 3D-derived LAV was moderate. For M-mode, this may reflect the overall smaller mean volumes where a greater SD would incur a higher CV. The variability for 2D-derived LAV was generally lower than both 1D and 3D methodologies. In general the CV between left- and right-sided methods was not systematically different.

Table 14: Interobserver variability for 3 phases of atrial function

Variable	**SD**	**Mean**	**CV**
2D RSA cube-r	5.16	22.72	23%
2D RSA sphere-r	2.70	11.89	23%
2D RSA cube-c	4.42	18.12	24%
2D RSA sphere-c	2.31	9.49	24%
2D RSA cube-s	2.78	11.21	25%
2D RSA sphere-s	1.46	5.87	25%
2D RLA MOD-r	2.40	27.29	9%
2D RLA ALM-r	2.55	29.33	9%
2D RLA MOD-c	2.67	21.20	13%
2D RLA ALM-c	3.09	22.63	14%
2D RLA MOD-s	1.97	14.02	14%
2D RLA ALM-s	2.14	15.10	14%
2D LAP MOD-r	2.69	25.24	11%
2D LAP ALM-r	2.91	27.24	11%
2D LAP MOD-c	2.10	18.52	11%
2D LAP ALM-c	1.82	19.99	9%
2D LAP MOD-s	2.00	12.32	16%
2D LAP ALM-s	2.31	13.31	17%
3D RLA-r	2.57	21.47	12%
3D RLA-c	2.38	15.94	15%
3D RLA-s	1.49	11.21	13%
3D LAP-r	2.98	20.37	15%

3D LAP -c	2.28	15.03	15%
3D LAP -s	1.43	11.16	13%
3D Biplane-r	3.44	21.26	16%
3D Biplane-c	2.06	16.28	13%
3D Biplane-s	2.01	11.86	17%
2D Biplane-r	3.14	24.30	13%
2D Biplane-c	1.91	17.75	11%
2D Biplane-s	1.00	12.83	8%
MM cube	1.17	7.90	15%
MM sphere	0.61	4.13	15%

Image quality analysis:

For right-sided 2D images, 31 dogs had excellent image quality and 9 dogs had acceptable images. For left-sided 2D images, 6 dogs had excellent image quality, 12 dogs had acceptable images, and 22 dogs had marginal image quality. For right-sided 3D images, 23 dogs had excellent image quality, 12 dogs had acceptable images, and 5 had marginal images. For left-sided 3D images, 8 dogs had excellent image quality, 16 dogs had acceptable images, and 16 had marginal images. Interestingly, image quality was notably better from the right-sided windows for 2D and 3D. The image quality was either marginal or acceptable on small dogs with 2D and 3D images from the right parasternal window. This reflects the difficulty noted by the echocardiographer in obtaining decent LA images from the right on smaller dogs. On the other end of the spectrum, image quality was worse overall (i.e. more marginal/acceptable scores) for large-breed dogs imaged from the left. This likely reflects the fact the LA is in the far field on the LAP view, making deep-chested or giant breed dogs challenging to accurately image from the left-sided window.

Discussion:

The results of our study support the hypothesis that RT3DE is a feasible, noninvasive method to measure LAV in a population of normal dogs. With regard to the different methods employed for LAV assessment, the 3D LAP had the strongest relationship to BW for all phases of the LA cycle. While this relationship was strong, it was imperfect and there are several reasonable explanations for this finding. Most intuitive is the fact that BW, nutritional status, and frame size have a dynamic relationship. Animals of the same BW may have very different frames (i.e. lean 15 kg whippet and obese 15kg rat terrier). As mentioned previously, documented somatotype was independent of BW for echocardiographic variables in one population of normal dogs.[59] Second, our study had several outliers, which may have been due to our generous inclusion criteria wherein dogs with historically larger hearts (e.g. greyhounds) were not excluded.[60,74]

Importantly, our data also suggests different methods of LA measurement are not all comparable. We found that converting the linear M-mode measurement to a volume via the cube or volume of a sphere formulas significantly underestimates LAV. Each 2D and 3D method used in this study was statistically different than LAV measured by M-mode (2D RLA MOD/ALM, 2D LAP MOD/ALM, 3D RLA/LAP, 2D and 3D Biplane = $p<0.0001$ compared to M-mode values). The discordance between 1D and 2D/3D LA size has been demonstrated in human and veterinary studies.[44] The significant underestimation of LAV via M-mode measurement is predictable, and can be explained by anatomic differences in how the measurement is obtained. M-mode techniques extrapolate volume from a single short-axis linear measurement. This measurement

involves dropping a fixed echobeam cursor in a straight line to bisect the aortic root and ideally the LA body. In normal dogs however, the cursor often bisects the cranial portion of LA body at best, or the LA appendage.[39] This is different from humans were the body of the LA is bisected.[36] The insonation angle therefore can significantly underestimate LA size. Anatomic M-mode may negate some of this inaccuracy however the processing software used to analyze our data did not allow for application of anatomic M-mode unfortunately. The authors conclude that M-mode should not be used to quantify LAV when 2D and 3D techniques are available.

Outside of the conclusions drawn about M-mode derived LAV, the results of our study indicate there were several pertinent differences between 2D and 3D methods of LAV analysis. The 3D-derived RLA-r was significantly less than the 2D-derived RLA MOD/ALM-r. This is likely due to the inferior temporal and spatial resolution of RT3DE. The 2D RLA MOD was significantly greater than the 2D-derived RSA LAV during all phases of the cardiac cycle, suggesting the volumes derived from the right-sided long axis view may not be equivalent to short axis volumes. The RSA cube and spheric LAV was significantly different for all phases of the LA cycle except the systolic phase, suggesting the cube and sphere formulas are not interchangeable. That the formulas differ is intuitive, the formula for the volume of a cube is mathematically distinct for the volume of a sphere. Our data indicates the resulting values are significantly different from each other. Furthermore, the 2D LAP MOD/ALM volumes were not significantly different than the LAV from the RSA cube formula for any phase of the cycle, whereas there were systematic differences identified when the RSA sphere formula was used. Importantly, 3D LAP was not significantly different than the 2D LAP MOD or the 2D biplane for any

phase of the cardiac cycle, yet differences were found when the 2D LAP ALM was used.

While the exact relationship between 2D and 3D echocardiography is uncertain, it is generally accepted that echocardiography systematically underestimates absolute LAV compared to MRI.[45] The explanation for this lies in the difference in spatial resolution between modalities. The greater resolution of MRI permits improved endocardial border detection. Loss of lateral image resolution is documented when imaging far field objects, which occurs when the LA is imaged from the LAP window. Even though echocardiography underestimates LAV compared to CT or MRI, echocardiography remains the least invasive, reliable, and cost-effective method to provide risk assessment and therapeutic trend information.

Evaluating the functional indices measured in this study suggest that the volume results are method-dependent. On the otherhand, the fractional indices often have similar results since the methodic bias present may effectively cancel out during calculation. In other words, smaller maximum and minimum volumes overall may result in similar ejection fractions compared to larger overall volumes. For the LAEF data, the average LAEF was approximately 50% using 6 different methods of LAV analysis. This value approximates the atrial emptying previously reported in an LA physiology study in dogs where total atrial emptying area was 50% at control conditions with normal atrial pressures.[11] In people normal LAEF ranges from 45-79% (95% confidence interval) with decent reproducibility.[75] In our study LAEF did not correlate with BW or $BW^{0.75}$. This would make sense logically since ejection fraction is also an indexed value and all of our subjects were healthy dogs.

There is little published for LAEF in dogs. One group evaluated LAEF in a population of normal dogs (*n*=52) and those affected with degenerative mitral valve disease (*n*=101). The median LAEF was 37.5% (IQR 29-48.8%) in the control group, which was not significantly different from the median LAEF of diseased dogs of 41.3% (IQR 31.9-52.7%).[72] The investigators did find that LAEF decreased as LA and LV volume increased in the absence of overt diastolic dysfunction, which may reflect deteriorating LA performance. The authors in that study did not subanalyze LAEF in the dogs with significant LA enlargement due to the small numbers in that particular group. LA contractile function is expected to initially improve with either increased volume or pressure load according to the Frank-Starling mechanism. However after this relationship peaks, pathologic myocyte stretch impairs atrial contraction. However these results are in contrast to another LAEF study in normal and diseased dogs, which found a negative correlation between LAEF and BW in control dogs, which could not be explained by HR in that study population. The absence of a correlation of LAEF to HR may be legitimate, or may reflect the population bias in this group of dogs since the median weight was relatively small at 17 kg with an interquartile range of 8.6-30.5 kg. Higher heart rates are associated with increased LAEF, and it is anecdotally thought that smaller dogs are permitted generally higher HR during an echocardiogram, whereas large-breed dogs may be less sympathetically driven to result in a lower overall HR. However this long-held dogma has been questioned by a recent large scale study where HR did not correlated with body size in a diverse population of dogs.[76]

No attempts were made to scientifically correlate heart rate (HR) with LA size or function in our study. Anecdotally however, we found that respiratory sinus arrhythmia

was particularly troublesome for RT3DE, resulting occasionally in software paralyzing stitching artifact and poor rendering of 3D volumes. The presence of tachycardia was also particularly challenging for 3DRTE analysis; discerning the separate phases of the LA cycle was nearly impossible in the setting of significant tachycardia (HR>140 beats per minute). This finding can be explained by the limited temporal resolution of RT3DE. For example, with a typical 2D frame rate of 100 frames per second and a HR of 60 beats per minute, each beat is comprised of 100 frames. With that same frame rate and a higher heart rate of 140 beats per minute, each beat is now comprised of 43 frames. Then combining a higher heart rate of 140 beats per minute with a typical lower 3D frame rate of 20 frames per second equals 8.6 frames per beat. The ability to discern maximal and minimal LAV with 8 frames to choose between is challenging and may result in erroneous data. We expect this issue will resolve in the future with the inevitable advancement of improvements in temporal resolution.

The interobserver variability results in this study suggest that amount of variability between observers for 3D LAV was acceptable. With the exception of the RSA measurements, the 2D measurements had lower CV values than their corresponding 3D measurements. While we hypothesized that LAV would be more reproducible with the benefit of 3D image acquisition, rather than reliance of monoplane or biplane 2D images, however this hypothesis was rejected by our data results. We also thought the slower 3D frame rates would decrease the CV since there would be less choices for frame selection, so 2 independent observers are more likely to pick the same frame. However this is tempered by the variability observers have in discriminating the 5 endocardial reference points and manual modification of the automatically generated cast.

Study limitations:

There are several noteworthy limitations to be mentioned. First and probably most importantly, our study did not involve comparison to a volumetric gold standard. Therefore our conclusions should not be extended to speculation of absolute LAV. Cardiac MRI is considered the non-invasive gold standard for chamber quantification; unfortunately its use in veterinary medicine is limited by the unavoidable necessity of general anesthesia. Looking to the future, a prospective study would involve CT or MRI LAV compared with 2D and 3D LAV, with LAV by echocardiography set as a dependent variable and LAV by a volumetric gold standard as the independent variable in a linear regression analysis.

Measurements were performed based on our description, however frame selection was dependent on image quality and frame rate. Therefore not all measurements were obtained at the same point within the cardiac cycle; this limitation was offset by the averaging of 3 measurements for each variable. Also a relatively small number of dogs were evaluated with liberal inclusion criteria and the data requires validation with larger cohorts. Heart rates, breed, age, sex, or fitness were not standardized. In people a breath hold is used during RT3DE data acquisition for each cardiac cycle, which was not possible with our unsedated study participants. This incurred significant stitching artifact with some study participants.

Despite conscientious attempts to minimize LAP foreshortening, underestimation of LAV due to foreshortening can be a potential source of error. Also it is technically difficult to confirm the 4- and 2-chamber views are truly orthogonal. Another source of

potential error occurred when the computer generated endocardial LA cast required manipulation in 100% of cases for both observers. This partially can be explained by the fact that the software is specifically designed for LV volume assessment, and may not have required as laborious emendation with the intended LV analysis. However this time commitment deserves specific mention, as a diagnostic tool must clear scrupulous standards to move from the research arena to clinical service. The authors expect the time necessary to modulate the image cast will decrease commensurately with improved temporal and spatial resolution of future generations of RT3DE. An atrial-specific tailored algorithm is also currently available (TomTech). Lastly, there is no consensus opinion regarding the relationship between linear cardiac dimensions and BW or BSA, which continues to be a source of animated discussion among veterinary cardiologists.

Conclusions:

The results of our study support the hypothesis that RT3DE is a feasible, noninvasive method to measure LAV in a population of normal dogs. Our study data indicates LAV obtained from the 4-chamber LAP view using RT3DE has the highest correlation with BW for all phases of the LA cycle, with acceptable but not ideal interobserver variability. It is also noteworthy that neither of the examiners had a great deal of experience with 3D echocardiography prior to the conduct of this study. M-mode significantly underestimates LAV with poor correlation to the indexed 2D and 3D parameters. The volume-based functional parameters were method-dependent and LAEF was approximately 50% with a large range in our population. The utility of RT3DE in cardiac dysfunction also merits further investigative process.

Bibliography:

1. Rosca M, Lancellotti P, Popescu BA, Pierard LA. Left atrial function: pathophysiology, echocardiographic assessment, and clinical applications. *Heart.* Dec 2011;97(23):1982-1989.
2. Qamruddin S, Shinbane J, Shriki J, Naqvi TZ. Left atrial appendage: structure, function, imaging modalities and therapeutic options. *Expert Rev Cardiovasc Ther.* Jan 2010;8(1):65-75.
3. Howard E, Miller M. *Miller's Anatomy Of The Dog.* 3 ed. St. Louis, MO: WB Sauder's company; 1993.
4. Chapel E, Russel D, Schober K. Partial pericardial defect with left auricular herniation in a dog with syncope. *J Vet Cardiol.* Jun 2014;16(2):133-139.
5. Ho SY, Cabrera JA, Sanchez-Quintana D. Left atrial anatomy revisited. *Circulation. Arrhythmia and electrophysiology.* Feb 2012;5(1):220-228.
6. Tabata T, Oki T, Yamada H, et al. Role of left atrial appendage in left atrial reservoir function as evaluated by left atrial appendage clamping during cardiac surgery. *The American journal of cardiology.* Feb 1 1998;81(3):327-332.
7. Davis CA, 3rd, Rembert JC, Greenfield JC, Jr. Compliance of left atrium with and without left atrium appendage. *The American journal of physiology.* Oct 1990;259(4 Pt 2):H1006-1008.
8. Hondo T, Okamoto M, Yamane T, et al. The role of the left atrial appendage. A volume loading study in open-chest dogs. *Jpn Heart J.* Mar 1995;36(2):225-234.
9. Brewer FC, Moise NS, Kornreich BG, Bezuidenhout AJ. Use of computed tomography and silicon endocasts to identify pulmonary veins with echocardiography. *Journal of veterinary cardiology : the official journal of the European Society of Veterinary Cardiology.* Mar 2012;14(1):293-300.
10. Verheule S, Wilson EE, Arora R, Engle SK, Scott LR, Olgin JE. Tissue structure and connexin expression of canine pulmonary veins. *Cardiovascular research.* Sep 2002;55(4):727-738.
11. Tsakiris AG, Padiyar R, Gordon DA, Lipton I. Left atrial size and geometry in the intact dog. *The American journal of physiology.* Feb 1977;232(2):H167-172.
12. Kittleson MD, Kienle RD. *Small animal cardiovascular disease.* St. Louis: Mosby; 1998.
13. Kittleson MD, Kienle RD. Small animal cardiovascular medicine. St. Louis: Mosby; 1998:124.
14. Kojima T, Kawasaki M, Tanaka R, et al. Left atrial global and regional function in patients with paroxysmal atrial fibrillation has already been impaired before enlargement of left atrium: velocity vector imaging echocardiography study. *Eur Heart J Cardiovasc Imaging.* Mar 2012;13(3):227-234.
15. Hoit BD, Shao Y, Gabel M, Walsh RA. In vivo assessment of left atrial contractile performance in normal and pathological conditions using a time-varying elastance model. *Circulation.* Apr 1994;89(4):1829-1838.

16. Stefanadis C, Dernellis J, Toutouzas P. A clinical appraisal of left atrial function. *European heart journal.* Jan 2001;22(1):22-36.
17. Kagawa K, Arakawa M, Miwa H, et al. [Left atrial function during left ventricular diastole evaluated by left atrial angiography and left ventriculography]. *J Cardiol.* Jul-Aug 1994;24(4):317-325.
18. Blume GG, McLeod CJ, Barnes ME, et al. Left atrial function: physiology, assessment, and clinical implications. *European journal of echocardiography : the journal of the Working Group on Echocardiography of the European Society of Cardiology.* Jun 2011;12(6):421-430.
19. Abhayaratna WP, Seward JB, Appleton CP, et al. Left atrial size: physiologic determinants and clinical applications. *Journal of the American College of Cardiology.* Jun 20 2006;47(12):2357-2363.
20. Casaclang-Verzosa G, Gersh BJ, Tsang TS. Structural and functional remodeling of the left atrium: clinical and therapeutic implications for atrial fibrillation. *Journal of the American College of Cardiology.* Jan 1 2008;51(1):1-11.
21. Appleton CP, Galloway JM, Gonzalez MS, Gaballa M, Basnight MA. Estimation of left ventricular filling pressures using two-dimensional and Doppler echocardiography in adult patients with cardiac disease. Additional value of analyzing left atrial size, left atrial ejection fraction and the difference in duration of pulmonary venous and mitral flow velocity at atrial contraction. *Journal of the American College of Cardiology.* Dec 1993;22(7):1972-1982.
22. Kittleson MD, Brown WA. Regurgitant fraction measured by using the proximal isovelocity surface area method in dogs with chronic myxomatous mitral valve disease. *Journal of veterinary internal medicine / American College of Veterinary Internal Medicine.* Jan-Feb 2003;17(1):84-88.
23. Yoshida N, Okamoto M, Makita Y, Nanba K, Yoshizumi M. Determinants of enhanced left atrial active emptying with aging: left atrial preload, contractility or both? *Intern Med.* 2009;48(12):987-992.
24. Huston TP, Puffer JC, Rodney WM. The athletic heart syndrome. *The New England journal of medicine.* Jul 4 1985;313(1):24-32.
25. Erol MK, Ugur M, Yilmaz M, Acikel M, Sevimli S, Alp N. Left atrial mechanical functions in elite male athletes. *The American journal of cardiology.* Oct 15 2001;88(8):915-917, A919.
26. Toutouzas K, Trikas A, Pitsavos C, et al. Echocardiographic features of left atrium in elite male athletes. *The American journal of cardiology.* Dec 1 1996;78(11):1314-1317.
27. Gerstenblith G, Frederiksen J, Yin FC, Fortuin NJ, Lakatta EG, Weisfeldt ML. Echocardiographic assessment of a normal adult aging population. *Circulation.* Aug 1977;56(2):273-278.
28. Borgarelli M, Savarino P, Crosara S, et al. Survival characteristics and prognostic variables of dogs with mitral regurgitation attributable to myxomatous valve disease. *Journal of veterinary internal medicine / American College of Veterinary Internal Medicine.* Jan-Feb 2008;22(1):120-128.

29. Lord P, Hansson K, Kvart C, Haggstrom J. Rate of change of heart size before congestive heart failure in dogs with mitral regurgitation. *The Journal of small animal practice.* Apr 2010;51(4):210-218.
30. Reynolds CA, Brown DC, Rush JE, et al. Prediction of first onset of congestive heart failure in dogs with degenerative mitral valve disease: the PREDICT cohort study. *Journal of veterinary cardiology : the official journal of the European Society of Veterinary Cardiology.* Mar 2012;14(1):193-202.
31. Thomas WP, Gaber CE, Jacobs GJ, et al. Recommendations for standards in transthoracic two-dimensional echocardiography in the dog and cat. Echocardiography Committee of the Specialty of Cardiology, American College of Veterinary Internal Medicine. *J Vet Intern Med.* Jul-Aug 1993;7(4):247-252.
32. Thomas WP, Gaber CE, Jacobs GJ, et al. Recommendations for standards in transthoracic two-dimensional echocardiography in the dog and cat. Echocardiography Committee of the Specialty of Cardiology, American College of Veterinary Internal Medicine. *Journal of veterinary internal medicine / American College of Veterinary Internal Medicine.* Jul-Aug 1993;7(4):247-252.
33. Brown DJ, Rush JE, MacGregor J, Ross JN, Jr., Brewer B, Rand WM. M-mode echocardiographic ratio indices in normal dogs, cats, and horses: a novel quantitative method. *Journal of veterinary internal medicine / American College of Veterinary Internal Medicine.* Sep-Oct 2003;17(5):653-662.
34. Buck T. Basic principles and practical application. In: Buck T, Franke A, Monaghan MJ, eds. *Three-dimensional Echocardiography*. Berlin: Springer; 2011.
35. Roelandt JR, Kisslo J. Three-dimensional echocardiography: lessons in overcoming time and space. In: Buck T, Franke A, Monaghan MJ, eds. *Three-dimensional Echocardiography*. Berlin: Springer; 2011.
36. Manolio TA, Gottdiener JS, Tsang TS, Gardin JM. Left atrial dimensions determined by M-mode echocardiography in black and white older (> or =65 years) adults (The Cardiovascular Health Study). *The American journal of cardiology.* Nov 1 2002;90(9):983-987.
37. Cornell CC, Kittleson MD, Della Torre P, et al. Allometric scaling of M-mode cardiac measurements in normal adult dogs. *Journal of veterinary internal medicine / American College of Veterinary Internal Medicine.* May-Jun 2004;18(3):311-321.
38. Hansson K, Haggstrom J, Kvart C, Lord P. Left atrial to aortic root indices using two-dimensional and M-mode echocardiography in cavalier King Charles spaniels with and without left atrial enlargement. *Veterinary radiology & ultrasound : the official journal of the American College of Veterinary Radiology and the International Veterinary Radiology Association.* Nov-Dec 2002;43(6):568-575.
39. Rishniw M, Erb HN. Evaluation of four 2-dimensional echocardiographic methods of assessing left atrial size in dogs. *Journal of veterinary internal*

medicine / American College of Veterinary Internal Medicine. Jul-Aug 2000;14(4):429-435.

40. Tidholm A, Bodegard-Westling A, Hoglund K, Ljungvall I, Haggstrom J. Comparisons of 2- and 3-dimensional echocardiographic methods for estimation of left atrial size in dogs with and without myxomatous mitral valve disease. *Journal of veterinary internal medicine / American College of Veterinary Internal Medicine.* Nov-Dec 2011;25(6):1320-1327.
41. Suh IW, Song JM, Lee EY, et al. Left atrial volume measured by real-time 3-dimensional echocardiography predicts clinical outcomes in patients with severe left ventricular dysfunction and in sinus rhythm. *Journal of the American Society of Echocardiography : official publication of the American Society of Echocardiography.* May 2008;21(5):439-445.
42. Lang RM, Bierig M, Devereux RB, et al. Recommendations for chamber quantification: a report from the American Society of Echocardiography's Guidelines and Standards Committee and the Chamber Quantification Writing Group, developed in conjunction with the European Association of Echocardiography, a branch of the European Society of Cardiology. *Journal of the American Society of Echocardiography : official publication of the American Society of Echocardiography.* Dec 2005;18(12):1440-1463.
43. Stefano GT, Zhao H, Schluchter M, Hoit BD. Assessment of echocardiographic left atrial size: accuracy of M-mode and two-dimensional methods and prediction of diastolic dysfunction. *Echocardiography.* Apr 2012;29(4):379-384.
44. Lester SJ, Ryan EW, Schiller NB, Foster E. Best method in clinical practice and in research studies to determine left atrial size. *The American journal of cardiology.* Oct 1 1999;84(7):829-832.
45. Artang R, Migrino RQ, Harmann L, Bowers M, Woods TD. Left atrial volume measurement with automated border detection by 3-dimensional echocardiography: comparison with Magnetic Resonance Imaging. *Cardiovasc Ultrasound.* 2009;7:16.
46. Kataoka A, Funabashi N, Takahashi A, et al. Quantitative evaluation of left atrial volumes and ejection fraction by 320-slice computed-tomography in comparison with three- and two-dimensional echocardiography: a single-center retrospective-study in 22 subjects. *Int J Cardiol.* Nov 17 2011;153(1):47-54.
47. Valocik G, Druzbacka L, Valocikova I, Mitro P. Velocity vector imaging to quantify left atrial function. *Int J Cardiovasc Imaging.* Aug 2010;26(6):641-649.
48. Ujino K, Barnes ME, Cha SS, et al. Two-dimensional echocardiographic methods for assessment of left atrial volume. *The American journal of cardiology.* Nov 1 2006;98(9):1185-1188.
49. Pritchett AM, Jacobsen SJ, Mahoney DW, Rodeheffer RJ, Bailey KR, Redfield MM. Left atrial volume as an index of left atrial size: a population-based study. *Journal of the American College of Cardiology.* Mar 19 2003;41(6):1036-1043.

50. Wang Y, Gutman JM, Heilbron D, Wahr D, Schiller NB. Atrial volume in a normal adult population by two-dimensional echocardiography. *Chest.* Oct 1984;86(4):595-601.
51. Vandenberg BF, Weiss RM, Kinzey J, et al. Comparison of left atrial volume by two-dimensional echocardiography and cine-computed tomography. *The American journal of cardiology.* Apr 1 1995;75(10):754-757.
52. Maddukuri PV, Vieira ML, DeCastro S, et al. What is the best approach for the assessment of left atrial size? Comparison of various unidimensional and two-dimensional parameters with three-dimensional echocardiographically determined left atrial volume. *Journal of the American Society of Echocardiography : official publication of the American Society of Echocardiography.* Aug 2006;19(8):1026-1032.
53. Miyasaka Y, Tsujimoto S, Maeba H, et al. Left atrial volume by real-time three-dimensional echocardiography: validation by 64-slice multidetector computed tomography. *Journal of the American Society of Echocardiography : official publication of the American Society of Echocardiography.* Jun 2011;24(6):680-686.
54. Keller AM, Gopal AS, King DL. Left and right atrial volume by freehand three-dimensional echocardiography: in vivo validation using magnetic resonance imaging. *European journal of echocardiography : the journal of the Working Group on Echocardiography of the European Society of Cardiology.* Mar 2000;1(1):55-65.
55. Soliman OI, Krenning BJ, Geleijnse ML, et al. Quantification of left ventricular volumes and function in patients with cardiomyopathies by real-time three-dimensional echocardiography: a head-to-head comparison between two different semiautomated endocardial border detection algorithms. *Journal of the American Society of Echocardiography : official publication of the American Society of Echocardiography.* Sep 2007;20(9):1042-1049.
56. Meyer J, Wefstaedt P, Dziallas P, Beyerbach M, Nolte I, Hungerbuhler SO. Assessment of left ventricular volumes by use of one-, two-, and three-dimensional echocardiography versus magnetic resonance imaging in healthy dogs. *American journal of veterinary research.* Sep 2013;74(9):1223-1230.
57. Spencer KT, Mor-Avi V, Gorcsan J, 3rd, et al. Effects of aging on left atrial reservoir, conduit, and booster pump function: a multi-institution acoustic quantification study. *Heart.* Mar 2001;85(3):272-277.
58. Lombard CW. Normal values of the canine M-mode echocardiogram. *American journal of veterinary research.* Oct 1984;45(10):2015-2018.
59. Morrison SA, Moise NS, Scarlett J, Mohammed H, Yeager AE. Effect of breed and body weight on echocardiographic values in four breeds of dogs of differing somatotype. *Journal of veterinary internal medicine / American College of Veterinary Internal Medicine.* Jul-Aug 1992;6(4):220-224.
60. della Torre PK, Kirby AC, Church DB, Malik R. Echocardiographic measurements in greyhounds, whippets and Italian greyhounds--dogs with a

similar conformation but different size. *Australian Veterinary Journal.* Jan 2000;78(1):49-55.
61. Price GS, Frazier DL. Use of body surface area (BSA)-based dosages to calculate chemotherapeutic drug dose in dogs: I. Potential problems with current BSA formulae. *Journal of veterinary internal medicine / American College of Veterinary Internal Medicine.* Jul-Aug 1998;12(4):267-271.
62. Gehan EA, George SL. Estimation of human body surface area from height and weight. *Cancer Chemother Rep.* Aug 1970;54(4):225-235.
63. Conklin PM. Body surface area in the infant rat. *Journal of applied physiology.* Aug 1975;39(2):335-336.
64. Buchanan JW, Bucheler J. Vertebral scale system to measure canine heart size in radiographs. *Journal of the American Veterinary Medical Association.* Jan 15 1995;206(2):194-199.
65. Jepsen-Grant K, Pollak ER, Johnson LR. Vertebral heart scores in eight breeds. *Vet Radiol Ultrasound.* 2013 2013;54(1):3-8.
66. Bavegems V, Van Caelenberg A, Duchateau L, Sys SU, Van Bree H, De Rick A. Vertebral heart size ranges specific for whippets. *Veterinary radiology & ultrasound : the official journal of the American College of Veterinary Radiology and the International Veterinary Radiology Association.* Sep-Oct 2005;46(5):400-403.
67. Kraetschmer S, Ludwig K, Meneses F, Nolte I, Simon D. Vertebral heart scale in the beagle dog. *The Journal of small animal practice.* May 2008;49(5):240-243.
68. Lamb CR, Tyler M, Boswood A, Skelly BJ, Cain M. Assessment of the value of the vertebral heart scale in the radiographic diagnosis of cardiac disease in dogs. *Vet Rec.* Jun 10 2000;146(24):687-690.
69. Lamb CR, Wikeley H, Boswood A, Pfeiffer DU. Use of breed-specific ranges for the vertebral heart scale as an aid to the radiographic diagnosis of cardiac disease in dogs. *Vet Rec.* Jun 9 2001;148(23):707-711.
70. Singh MK, Johnson LR, Kittleson MD, Pollard RE. Bronchomalacia in dogs with myxomatous mitral valve degeneration. *Journal of veterinary internal medicine / American College of Veterinary Internal Medicine.* Mar-Apr 2012;26(2):312-319.
71. Hollmer M, Willesen JL, Tolver A, Koch J. Left atrial volume and phasic function in clinically healthy dogs of 12 different breeds. *Veterinary journal.* Sep 2013;197(3):639-645.
72. Tidholm A, Hoglund K, Haggstrom J, Bodegard-Westling A, Ljungvall I. Left atrial ejection fraction assessed by real-time 3-dimensional echocardiography in normal dogs and dogs with myxomatous mitral valve disease. *Journal of veterinary internal medicine / American College of Veterinary Internal Medicine.* Jul-Aug 2013;27(4):884-889.
73. West GB, Brown JH, Enquist BJ. A general model for the origin of allometric scaling laws in biology. *Science.* Apr 4 1997;276(5309):122-126.
74. Lonsdale RA, Labuc RH, Robertson ID. Echocardiographic parameters in training compared with non-training greyhounds. *Veterinary radiology &*

ultrasound : the official journal of the American College of Veterinary Radiology and the International Veterinary Radiology Association. Jul-Aug 1998;39(4):325-330.

75. Aune E, Baekkevar M, Roislien J, Rodevand O, Otterstad JE. Normal reference ranges for left and right atrial volume indexes and ejection fractions obtained with real-time three-dimensional echocardiography. *European journal of echocardiography : the journal of the Working Group on Echocardiography of the European Society of Cardiology.* Aug 2009;10(6):738-744.
76. Lamb AP, Meurs KM, Hamlin RL. Correlation of heart rate to body weight in apparently normal dogs. *Journal of veterinary cardiology : the official journal of the European Society of Veterinary Cardiology.* Aug 2010;12(2):107-110.